

3-21-2013

# Depth-Resolved Cathodoluminescence of ThO<sub>2</sub>

Michael G. Lee

Follow this and additional works at: <https://scholar.afit.edu/etd>

Part of the [Nuclear Commons](#)

## Recommended Citation

Lee, Michael G., "Depth-Resolved Cathodoluminescence of ThO<sub>2</sub>" (2013). *Theses and Dissertations*. 936.  
<https://scholar.afit.edu/etd/936>

This Thesis is brought to you for free and open access by the Student Graduate Works at AFIT Scholar. It has been accepted for inclusion in Theses and Dissertations by an authorized administrator of AFIT Scholar. For more information, please contact [richard.mansfield@afit.edu](mailto:richard.mansfield@afit.edu).



**DEPTH-RESOLVED CATHODOLUMINESCENCE OF THORIUM DIOXIDE**

THESIS

Michael G. Lee, Major, USA

AFIT-ENP-13-M-21

**DEPARTMENT OF THE AIR FORCE  
AIR UNIVERSITY**

**AIR FORCE INSTITUTE OF TECHNOLOGY**

---

---

**Wright-Patterson Air Force Base, Ohio**

**DISTRIBUTION STATEMENT A.  
APPROVED FOR PUBLIC RELEASE; DISTRIBUTION UNLIMITED**

The views expressed in this thesis are those of the author and do not reflect the official policy or position of the United States Air Force, Department of Defense, or the United States Government. This material is declared a work of the U.S. Government and is not subject to copyright protection in the United States.

AFIT-ENP-13-M-21

DEPTH-RESOLVED CATHODOLUMINESCENCE OF THORIUM DIOXIDE

THESIS

Presented to the Faculty

Department of Engineering Physics

Graduate School of Engineering and Management

Air Force Institute of Technology

Air University

Air Education and Training Command

In Partial Fulfillment of the Requirements for the  
Degree of Master of Science in Nuclear Engineering

Michael G. Lee, BS

Major, USA

March 2013

**DISTRIBUTION STATEMENT A.**

APPROVED FOR PUBLIC RELEASE; DISTRIBUTION UNLIMITED

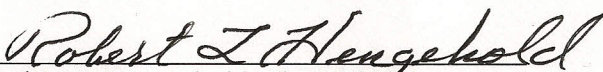
AFIT-ENP-13-M-21

DEPTH-RESOLVED CATHODOLUMINESCENCE OF THORIUM DIOXIDE

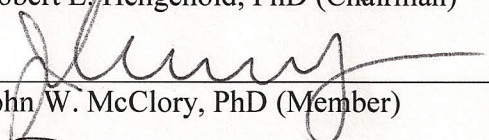
Michael G. Lee, BS

Major, USA

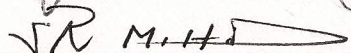
Approved:

  
\_\_\_\_\_  
Robert L. Hengehold, PhD (Chairman)

3/11/13  
Date

  
\_\_\_\_\_  
John W. McClory, PhD (Member)

3/11/13  
Date

  
\_\_\_\_\_  
Stephen R. McHale, LTC, PhD (Member)

3/11/13  
Date

### Abstract

Single crystal, hydrothermally grown, thorium dioxide ( $\text{ThO}_2$ ) samples were studied using depth-resolved cathodoluminescence (CL) to characterize the surface and bulk electronic states. X-ray diffraction (XRD) measurements were collected to confirm that these crystals were  $\text{ThO}_2$  in the fluorite structure. Understanding the chemical and structural quality of  $\text{ThO}_2$  will aid in the fabrication of better neutron detectors as well as in the power production with thorium breeder reactors.

Monte Carlo simulations using CASINO were used to predict the expected energy-dependent electron interaction depths in the  $\text{ThO}_2$  crystals. CL was conducted with an electron energy range of 1.5 - 12 keV, a current range of 30-62  $\mu\text{A}$ , in vacuums of  $5 \times 10^{-7}$  to  $1.2 \times 10^{-9}$  Torr, and sample temperatures of 24 K – 297 K. The initial CL measurements indicated that the as-grown sample exhibited more of an energy dependency than the cut and polished sample. However, in a companion study, time of flight secondary ion mass spectrometry (TOF SIMS) was conducted on the samples. In the process, the sample surfaces were partially cleaned. Additional CL measurements were conducted on both samples after their inadvertent cleaning, which indicated that the as-grown sample no longer exhibited the observed energy dependency.

Deconvolution of the CL spectra indicated that there were five peaks that made up the CL spectra in all cases. One of these peaks was the band edge luminescence at 5.1 eV which was confirmed with transmittance measurements which indicated the existence of an absorption edge near 5.4 eV.

AFIT-ENP-13-M-21

*To my loving Wife*

## Acknowledgments

First, I acknowledge Jesus Christ for providing me this Great Adventure of Graduate School and an opportunity to glorify Him upon successful completion of this mission. Second, I thank my Wife for supporting me 100% and giving me the gift of time to study hard. Next, I thank my Advisor—Dr. Robert L. Hengehold for his vigor, excitement, and patience in the experimental physics world of cathodoluminescence. U.S. Army Lieutenant Colonels McClory and McHale were always helpful with Additional Instruction on physics, CL software, and military professional matters. Mr. Tony Kelly was an invaluable contribution to making this report possible as he and I collaborated quite a bit to solve this ThO<sub>2</sub> problem. Dr. Alex Li helped confirm the surface quality of the crystals with the Atomic Force Microscope images he took.

Without the instrumentation expertise and many long, dedicated hours of lab assistance from Mr. Gregory Smith and Mr. Mike Ranft, I think I would be still taking data now! The great men of the AFIT fabrication shop—Mr. Brian Crabtree, Mr. Dan Ryan, and Mr. Chris Harkless—this thesis would not exist without their hard work. I thank my Ranger Buddy—Capt Jon D. Rowland—who is a great family friend, dedicated PT buddy, and an outstanding officer and a gentleman. I thank my mentor and friend—LTC Anthony J. Buetti—for always guiding me through life with his wisdom. Last but not least, I thank my Little Sister for always rooting for me in all my endeavors. RLW!

Michael G. Lee



## Table of Contents

	Page
Abstract.....	v
Acknowledgments.....	vii
List of Figures.....	x
List of Tables.....	xii
List of Abbreviations.....	xiii
I Introduction.....	1
1.1 Focus of Research.....	3
1.2 Document Structure.....	3
II Literature Review and Theory.....	4
2.1 Chapter Overview.....	4
2.2 ThO <sub>2</sub> and its Crystal Structure.....	4
2.3 Hydrothermal Crystal Growth Method.....	5
2.4 X-ray Diffraction (XRD).....	8
2.5 Cathodoluminescence (CL).....	10
2.6 Time of Flight Secondary Ion Mass Spectrometry (TOF SIMS).....	17
2.7 Atomic Force Microscope (AFM).....	17
2.8 Peak Fit 4.0.....	18
2.9 Optical Transmittance Measurement.....	18
2.10 Previous Luminescence Studies.....	19
III Experimental Set-Up and Materials Examined.....	22
3.1 Chapter Overview.....	22
3.2 CL Experimental Set-Up.....	22
3.3 ThO <sub>2</sub> sample investigated.....	31
IV Results and Analysis.....	33
4.1 Chapter Overview.....	33
4.2 CASINO Depth Penetration Simulation.....	33
4.3 ThO <sub>2</sub> Depth-Resolved CL.....	37
4.4 Post-TOF SIMS Measurements.....	51
4.5 Optical Transmittance Spectrum.....	66
V Conclusions and Recommendations for Future Research.....	68
5.1 CASINO.....	68
5.2 CL.....	68

5.3 Recommendations for Future Research .....	69
Appendix A: CL Start-up and Shut-down Procedures.....	70
Appendix B: ThO <sub>2</sub> Polished Sample, 10 and 5 keV Temperature Variation runs.....	73
Bibliography .....	75
Vita.....	79

## List of Figures

	Page
Figure 1. The ThO <sub>2</sub> fluorite structure.....	5
Figure 2. A schematic of the Tuttle cold seal and a view of the autoclave .....	6
Figure 3. Band heaters required to heat the ampoules up to 750°C.....	7
Figure 4. 2-Theta plot .....	9
Figure 5. The process of excitation and luminescence. ....	12
Figure 6. Different distributions of CASINO output of Z Max for silicon.....	14
Figure 7. A CASINO simulation of an arbitrary number of electrons.....	15
Figure 8. Cathodoluminescence Experimental Set-up.....	23
Figure 9. AFIT CL Experimental Diagram.....	24
Figure 10. ThO <sub>2</sub> and another sample mounted on a thin tantalum sheet. ....	25
Figure 11 A derivative of a model EMG-12 electron gun.....	26
Figure 12. COOLPOWER 4.2 GM Cryocooler.....	28
Figure 13. Optical diagram of SPEX 500M monochromator .....	29
Figure 14. PMT Housing .....	30
Figure 15. ThO <sub>2</sub> Sample #001TO .....	32
Figure 16. Polished ThO <sub>2</sub> Sample #004TO. ....	32
Figure 17. CASINO simulation with 20,000 electrons at beam energy of 7 keV .....	34
Figure 18. ZMax plot of 20,000 electrons of 5 keV energy. ....	35
Figure 19. CASINO simulation with 20,000 electrons at beam energy of 10 keV .....	36
Figure 20. ThO <sub>2</sub> #001TO irradiated with beam energy of 1.51 keV. ....	37
Figure 21. ThO <sub>2</sub> #001TO Energy Dependent Experiment at 192 K.....	38

Figure 22. At various temperatures, #001TO irradiated with a beam energy of 7 keV...	39
Figure 23. 24 K CL spectrum of ThO <sub>2</sub> #001TO using beam energy of 10 keV .....	40
Figure 24. Sample #001TO examined with 10 keV at low and room temperatures.....	41
Figure 25. Sample #001TO examined with 10 keV at intermediate temperatures.....	42
Figure 26. ThO <sub>2</sub> #001TO at various temperatures irradiated by beam energy 12 keV ...	43
Figure 27. ThO <sub>2</sub> #001TO Current Dependency study at 12 keV.....	45
Figure 28. An energy dependency study of ThO <sub>2</sub> #004TO at 27 K. ....	46
Figure 29. ThO <sub>2</sub> #004TO irradiated with beam energy of 7 keV .....	48
Figure 30. A closer 7 keV inspection of ThO <sub>2</sub> #004TO .....	49
Figure 31. TOF SIMS measurements .....	51
Figure 32. Atomic Force Microscope image of Polished ThO <sub>2</sub> .....	52
Figure 33. Post-TOF SIMS, As-Grown ThO <sub>2</sub> Energy Dependency Runs.....	53
Figure 34. Post-TOF SIMS, As-Grown ThO <sub>2</sub> Energy Dependency Runs.....	55
Figure 35. Post-TOF SIMS, Polished ThO <sub>2</sub> Energy Dependency Runs.....	56
Figure 36. Post-TOF SIMS, Polished ThO <sub>2</sub> irradiated with 1.5 keV beam energy.....	57
Figure 37. Post-TOF SIMS, Polished ThO <sub>2</sub> de-convolution .....	60
Figure 38. Zoomed-in depiction of the as-grown 12 keV.....	60
Figure 39. Post-TOF SIMS, Polished ThO <sub>2</sub> irradiated with 2.5 keV beam energy.....	62
Figure 40. Post-TOF SIMS, Polished ThO <sub>2</sub> de-convolution .....	63
Figure 41. Post-TOF SIMS ThO <sub>2</sub> Comparison.....	65
Figure 42. Optical Transmittance Spectrum at room temperature.....	66

## List of Tables

	Page
Table 1. Equipment Data for CL Components .....	24
Table 2. Expected Electron Interaction within ThO <sub>2</sub> .....	34
Table 3. Sample #001TO Energy Dependent Peak Locations at 192 K.....	38
Table 4. Sample #001TO Temperature Dependent Peak Locations at 7 keV. ....	39
Table 5. Sample #001TO Temperature Dependent Peak Locations at 10 keV. ....	42
Table 6. Sample #001TO Temperature Dependent Peak Locations at 12keV. ....	44
Table 7. Sample #004TO Energy Dependent Peak Locations at 27 K.....	47
Table 8. Sample #004TO Temperature Dependent Peak Location at 7 keV.....	49
Table 9. Post-TOF SIMS As-Grown ThO <sub>2</sub> Energy Dependent Peak Locations .....	54
Table 10. Post-TOF SIMS Polished ThO <sub>2</sub> Sample Energy Dependent Peak Locations, Peak-Fitted De-convolved Peak Locations with Wavelength Differences, and Regression Values. (1)-(5) denote the mini-peaks de-convolved. ....	59
Table 11. Peak Fit 4.0 Deconvolution of CL Peaks with 5-sub-peaks; the wavelength differences between each combination of fits based-off the shortest wavelength (band gap); and regression value of best-fit. ....	64

## List of Abbreviations

Abbreviation	Page
<sup>60</sup> C.....Carbon-60, Buckyball.....	62
<sup>233</sup> U.....Uranium-233.....	1
<sup>238</sup> Pu.....Plutonium-238.....	1
AFM.....Atomic Force Microscope.....	63
BE.....Back-scattered electrons.....	19
CASINO.....monte <u>C</u> arlo <u>S</u> imulation of electro <u>N</u> trajectory in s <u>O</u> lids.....	19
CL.....Cathodoluminescence.....	2
DHS.....Department of Homeland Security.....	1
EHP.....Electron-hole pairs.....	2
FCC.....Face-centered cubic.....	4
N <sub>2</sub> .....Nitrogen-2.....	30
OFHC.....Oxygen Free High Conductivity.....	29
PMT.....Photo-multiplier tube.....	25
SC.....Simple cubic.....	4
SR.....surface-recombination.....	26
ThO <sub>2</sub> .....Thorium dioxide.....	1
TOF SIMS.....Time of Flight Secondary Ion Mass Spectroscopy.....	62

# DEPTH-RESOLVED CATHODOLUMINESCENCE OF THORIUM DIOXIDE

## I Introduction

Nuclear weapon non-proliferation is a major goal of the world as there is a constant fear that terrorists could obtain the special nuclear material (SNM) to make their own weapons. The Department of Homeland Security (DHS) desires to create better neutron detectors to thwart terrorist activities. Detecting the radioactive decay products of the nuclear material prevents terrorists from transporting SNM. Also, as the world's energy demands continue to increase, new non-fossil fuel sources are being studied (Mann & Thompson, 2010). Thorium dioxide ( $\text{ThO}_2$ ) is an emerging energy option to produce nuclear energy as well as for use in neutron detectors.

Thorium can absorb a neutron and undergo two beta-decays to form fissionable uranium-233 ( $^{233}\text{U}$ ). Thorium is resistant to nuclear weapons proliferation because unlike natural uranium, natural thorium contains only trace amounts of fissile material (such as thorium-231), which are insufficient to initiate a nuclear chain reaction. The thorium fuel cycle produces only small amounts of  $^{235}\text{U}$ , which is a key isotope of uranium used in the development of plutonium-239 ( $^{239}\text{Pu}$ )-based nuclear weapons. Thorium also results in less highly radioactive waste in comparison to the uranium fuels.

Thorium is four times more plentiful in the earth's crust than uranium, and it does not need isotopic enrichment before use (Martin & Cooke, 2012). For example, over the

past few decades, India has been researching thorium. India has approximately 290,000 tons of economically extractable thorium (Maitura, 2005). Globally, there is sufficient thorium to provide the world's energy needs for several thousand years (Martin & Cooke, 2012). As a result, since the uranium reserves around the world are decreasing, the thorium fuel cycle is becoming a cost-effective material for supplying future power needs.

The thorium fuel is likely to take the form of  $\text{ThO}_2$  or  $\text{ThO}_2$  with uranium added to it (uranium-doped) when it is used in reactors. The fertile  $^{232}\text{Th}$  is converted into fissile  $^{233}\text{U}$ , with the fuel elements remaining within the reactor cores for years rather than months, as is the case with conventional uranium fuel (Martin & Cooke, 2012). A full understanding of the material properties of thorium and its performance in intense radiation fields is essential. A quality depth-resolved CL study is a method to ultimately ensure that we can utilize thorium as a potentially safer and more sustainable fuel. In this study, luminescence spectroscopy, particularly CL, will be utilized to evaluate the quality of the undoped  $\text{ThO}_2$  crystals produced by hydrothermal growth. This method was chosen because it is capable of producing large single crystals that can be mounted for cathodoluminescence (CL) experiments. CL is sensitive to the presence of defects, and the energy of the electrons of the excitation beam can be varied. The flexibility of varying the electron beam energies allows for easy examination of the material at different depths into the material determined by the beam energy.



## 1.1 Focus of Research

This study seeks to characterize ThO<sub>2</sub> via CL. The CL spectra will explain how hydrothermally grown ThO<sub>2</sub> behaves electronically in both the surface and bulk. The quality of the samples will be observed by conducting an in-depth energy and temperature dependence study. This study will also address the band gap for this hydrothermally grown ThO<sub>2</sub> crystal.

## 1.2 Document Structure

This document is arranged into five chapters. Chapter II provides background for the study. It will cover the properties and crystal structure of ThO<sub>2</sub>, ThO<sub>2</sub> hydrothermal growth, X-Ray Diffraction (XRD), CL, Atomic Force Microscopy (AFM), Time of Flight Secondary Ion Mass Spectrometry (TOF SIMS), the optical transmittance measurement, and previous luminescence studies of ThO<sub>2</sub>. Chapter III details the material used and explains the experimental set-up that will be used to obtain the data for this study. Chapter IV includes the results and analysis, which are followed by the conclusions and recommendations for future research in Chapter V.

## II Literature Review and Theory

### 2.1 Chapter Overview

This chapter will first present ThO<sub>2</sub>, its properties, and crystal structure. Next, the hydrothermal growth method will be covered followed by XRD that indicated a high degree of crystallinity for the hydrothermally grown ThO<sub>2</sub> crystal. The primary experimental technique—CL—will be described as well as a description of how the Atomic Force Microscope (AFM), Time of Flight Secondary Ion Mass Spectroscopy (TOF SIMS), and optical transmittance work. Lastly, previous luminescence studies on ThO<sub>2</sub> will be presented.

### 2.2 ThO<sub>2</sub> and its Crystal Structure

First, it is instrumental to develop an understanding of the physical properties of ThO<sub>2</sub>. Thorium is an actinide, and filling the unfilled 4f electronic orbit shell is the high interest for experimenters today. This study looked at an oxide of an actinide. ThO<sub>2</sub> is depicted in Figure 1. The oxygen atoms are arranged in the face-centered cubic (FCC) structure, whereas the thorium atoms are in the simple cubic (SC) structure (Fluorite-unit, 2012). Thorium-232 is one of two naturally found actinides in the earth, where the other element is uranium-235. All the other actinides are created in scientific laboratories.

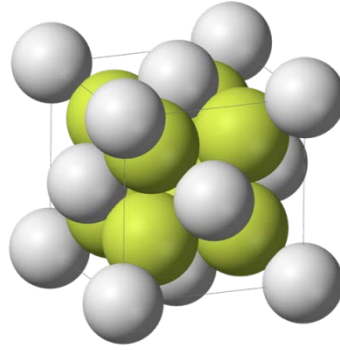


**Figure 1. The ThO<sub>2</sub> fluorite structure (Fluorite-unit, 2012).**

### **2.3 Hydrothermal Crystal Growth Method**

The ThO<sub>2</sub> crystals used in this study were grown by the hydrothermal low temperature growth technique, where it mimics the naturally occurring mineral formation from an aqueous solution. The ThO<sub>2</sub> crystals used in this study were grown by Dr. James M. Mann at Clemson University (Mann M. J., 2009). This technique performs crystal growth between 100°C and 800°C in an aqueous solution, typically water, contained in a closed vessel. Hydrothermal synthesis is known to induce very few crystalline defects in the final crystal; however, this is tempered by the disadvantage of its slow growth rate. The small growth rates necessitate a significant time investment for industrial growth of large single crystals.

Spontaneous nucleation reactions were performed in silver ampoules of various lengths (2-8") and diameters (1/4 – 3/8") (Mann & Thompson, 2010). The 99.99% ThO<sub>2</sub> powder was placed into the ampoule with a basic mineralizer such as cesium fluoride. The ampoule was then welded shut as seen in Figure 2. The mineralizer was loaded into the ampoule in its solid form, and then using a syringe, deionized water was added to

reach the desired concentration. The ampoules were then placed in a 27 mL internal volume Inconel autoclave with the remaining volume filled with water to provide counter-pressure (Mann & Thompson, 2010). Once the mineralizer and reactants were loaded, the open end of the ampoule was crimped and then welded shut.

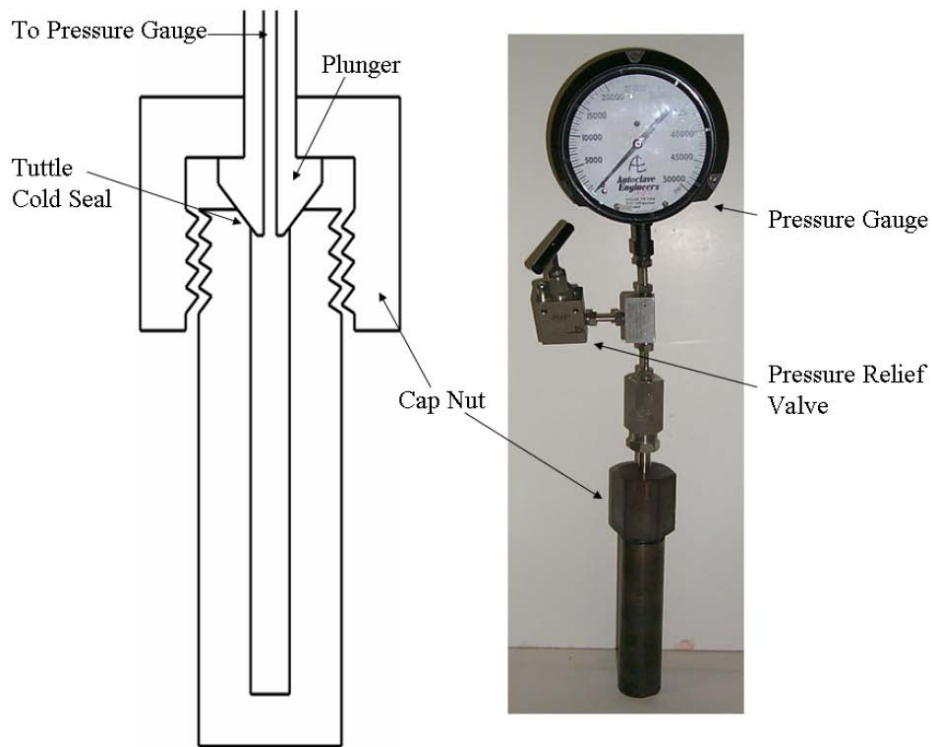


**Figure 2.** A schematic of the Tuttle cold seal and a view of the autoclave with the head assembly. Adopted from (Mann M. J., 2009). Permission granted by Dr. Mann on 27 FEB 2013 to use these diagrams from his PhD dissertation, Clemson University, Department of Material Sciences.

The vessel was then heated to temperatures between 400°C and 750°C, which generated pressures between 10 and 30 kpsi (Mann & Thompson, 2010). A seed crystal of ThO<sub>2</sub> was drilled and hung from a ladder using 0.1 mm silver wire (Mann & Thompson, 2010). In Figure 2, a typical autoclave is depicted, and it can withstand temperatures of 800°C and extremely high pressures. Before attaching the plunger, pressure relief valve, and the pressure gauge, water was added to the remaining internal

volume of the autoclave to act as counter pressure. This prevents the silver ampoules from bursting when heated. Band heaters enable the autoclave to reach synthesis temperatures as shown in Figure 3.

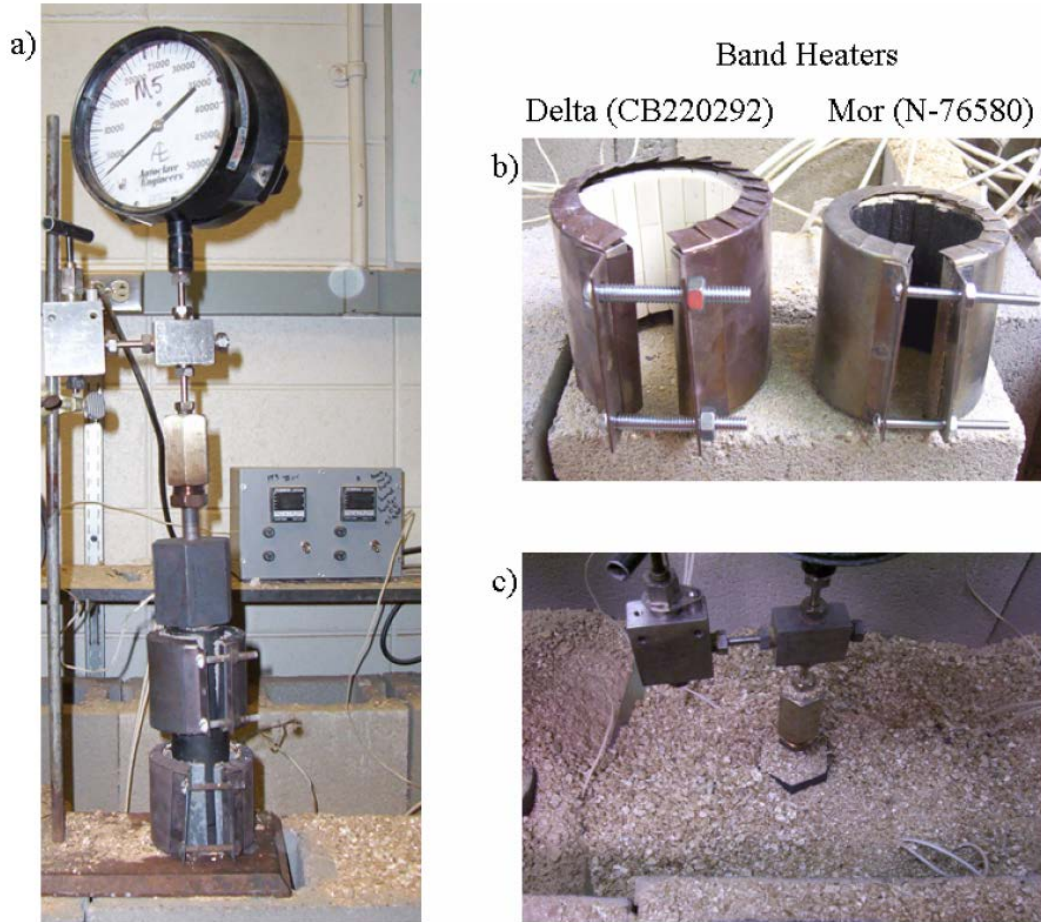


**Figure 3. Band heaters required to heat the ampoules up to 750°C (Mann M. J., 2009). Permission granted by Dr. Mann on 27 FEB 2013 to use these diagrams from his PhD dissertation, Clemson University, Department of Material Sciences.**

Once the aforementioned components are assembled on top of the autoclave, a tight Tuttle cold seal is formed as shown in Figure 2. The synthesis temperature is within the range of 400°-750°C, where these temperatures generate high pressures. Reactions are held at temperature generally between 5-21 days. The autoclave is then cooled to

room temperature and opened. In order to form crystals larger than 1 mm in length, transport growth experiments are performed. Seed crystals of approximately 3 mm in size must be used, and they can be formed from spontaneous nucleation reactions. ThO<sub>2</sub> is formed by using seed crystals, and it grew 1 mm/week (Mann M. J., 2009). Although these ThO<sub>2</sub> samples are single crystals, there are defects.

## 2.4 XRD

XRD, or X-ray diffraction, is a versatile, non-destructive technique that can be utilized to reveal information about the chemical composition and crystallographic structure of ThO<sub>2</sub>. Diffraction can indirectly reveal details of the internal structure of the order of 10<sup>-8</sup> cm in size (Cullity, 1956). Diffraction is the result of electromagnetic waves starting out in phase and rejoining with some phase difference, usually the result of the waves having different optical path lengths before rejoining. If the path length is different by an integer wavelength, the waves will still be in phase.

The atoms that comprise the crystal will scatter the incident x-rays in all directions, with some directions producing beams that are in phase. The condition that produces rays that are completely in phase is the Bragg law:

$$n\lambda = 2d \sin\theta, \quad (1)$$

with  $\theta$  being the angle of incidence and  $d$  being distance between planes in the crystal;  $n$  is the order of reflection which may be any integral value that does not force  $\sin(\theta)$  to be greater than unity. Waves that are out of phase will cause destructive interference, thus annulling one another. Constructive interference, therefore, can only occur at certain angles of incidence. If the wavelength is fixed, and the x-ray scans over  $\theta$ , the lattice

spacing can be determined for a given axis of rotation of the crystal. This is known as the rotating-crystal method. One can then determine the structure of the crystal based on the angles that cause diffraction.

Powder XRD of  $\text{ThO}_2$  is presented in the upper spectrum of Figure 4. The lower histogram peaks were taken from the ICSD (Inorganic Crystal Structure Database) (Karlsruhe, 2013). The positions and relative intensities of the peak match the reference powder diffraction profile for  $\text{ThO}_2$  (Castilow, 2012).

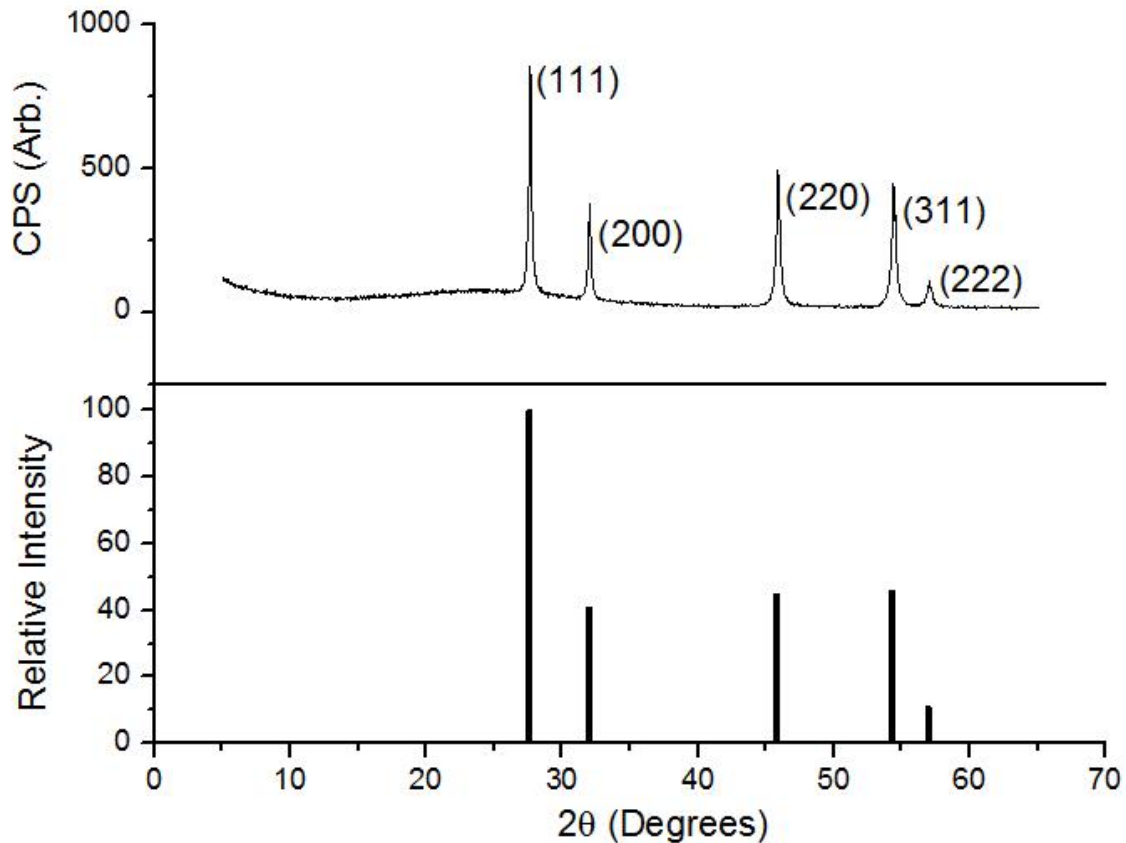


Figure 4. 2-Theta plotted by Jacob Castilow,  $\text{ThO}_2$  crystal grower, ENP Student. The upper XRD measurement was conducted by Dr. Matthew Mann. Permission granted by Dr. Mann via email on 27 FEB 2013 for the use of plot from his PhD dissertation.

ThO<sub>2</sub> is only known to have the fluorite phase. To identify a crystal structure, the peaks in the XRD spectrum should identify with the several peaks that are contained in the powder diffraction profile. Therefore, the sharp diffraction peaks emitted from the (111), (200), (220), (311), and (222) planes indicate a crystal in the fluorite structure possessing a high degree of crystallinity.

## 2.5 Cathodoluminescence (CL)

CL is the primary experimental technique used in this study. The basis of this technique is based upon the fact that when atoms in a crystal are excited by high energy electron beams, electrons in these atoms are excited to higher energy states. Subsequently, the atoms emit light by spontaneous emission when electrons in these excited states drop down to lower energy states by radiative transitions (Fox, 2010). In solids, the radiative emission process is called luminescence. Luminescence emission involves radiative transitions between electronic energy levels of the material and an emission is characteristic of the material (Lumb, 1978, Nomura, 2003). Since the intensity of the luminescence depends on the number of excited states which are populated, one focus will be on understanding how the excited electronic levels can be populated allowing one to study and characterize the undoped ThO<sub>2</sub> (Lumb, 1978, Nomura, 2003).

The basic processes that occur when an electron beam strikes a crystal are depicted in Figure 5. For example, at low temperatures and in the absence of any exciting mechanism, level zero (top of the valence band) alone is occupied. After



excitation, level five can be occupied. Because levels two to five are close together, the excitation can drop to level two by a non-radiative cascade process. If the gap between level two and the next lower level is large enough, the excitation in level two cannot be dissipated non-radiatively. With such a large gap the transition from level two to level one or zero may occur radiatively by emission of a photon of electromagnetic radiation, that is, by the emission of luminescence (Lumb, 1978).

Many possible electron energy levels exist within the forbidden gap, which is between  $E_0$  (top of the valence band) and  $E_2$  (defined as the bottom of conduction band) in Figure 5. Luminescence then occurs when an electron becomes excited to one of these levels and relaxes to recombine back at  $E_0$ . The full band gap transition will exhibit the maximum energy photon at a certain sample temperature. The band gap energy decreases as a function of increasing sample temperature since the interatomic spacing increases with temperature due to linear expansion of  $\text{ThO}_2$ . An increased interatomic spacing decreases the average potential seen by electrons in  $\text{ThO}_2$ , which in turn decreases the band gap.

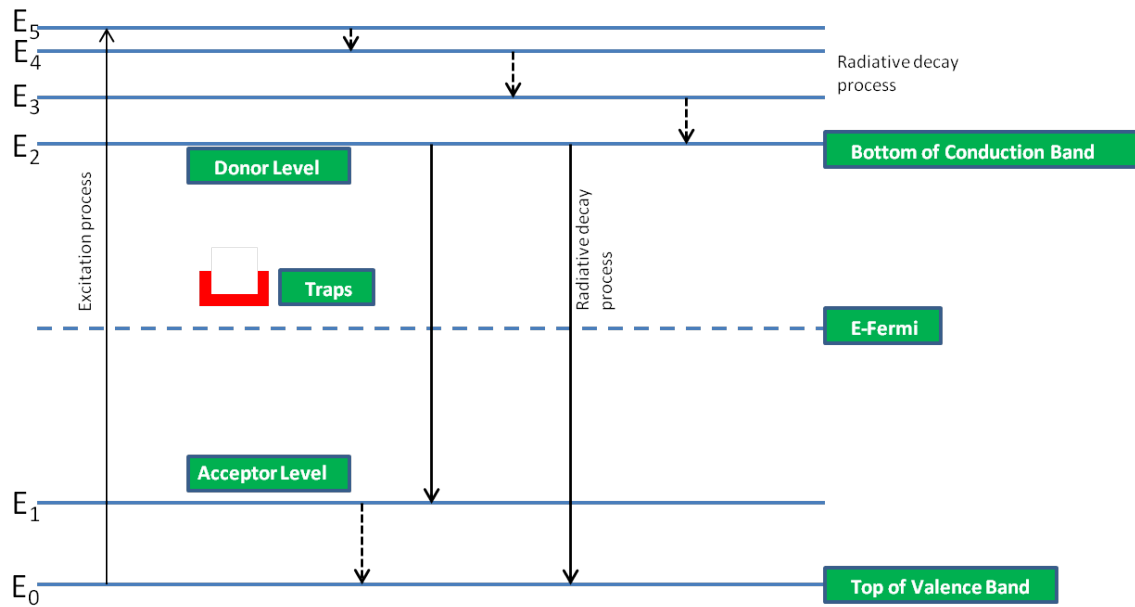


**Figure 5. The process of excitation and luminescence.**

Another exciting mechanism is when an electron becomes excited and relaxes down to a shallow donor level, close to the bottom of the conduction band. If  $\text{ThO}_2$  had been unintentionally doped with n-type materials, then the material would exhibit photons with an energy that is less than the band gap energy—photons resulting from electrons recombining from the donor level to  $E_0$ . Electrons may become trapped deep near E-fermi and then recombine at  $E_0$  as temperature changes. Or electrons could travel from the bottom of the conduction band to the acceptor level and emit a photon with a lesser energy than band gap energy. The objective of this report is to determine the different mechanisms occurring within the band gap of hydrothermally grown  $\text{ThO}_2$  as well as determine the full band gap.

The electrons in the electron beam are called primary electrons. They have an energy that is determined by the voltage applied to the electron gun, which is typically 1-

100 keV. The penetrating electrons lose their energy by elastic and inelastic collisions with the lattice ions along the electron trajectories, generating x-rays, Auger electrons, secondary electrons, EHPs, and phonons (Ozawa, 1990).

The production of BEs, X-ray emissions, and absorbed energy in the sample can be modeled by the “monte CARlo SIMulation of electroN trajectory in sOlids” (CASINO) Version 2.42 program (Drouin & Couture, 2007). CASINO allows for a good approximation of what the expected depth penetrations are for various electron gun energies applied to the sample. CASINO’s major assumption is that no relativistic effect has been included within the models since this effect will only start to be more important at higher energy (>50 keV) (Drouin & Couture, 2007). For this experimental study, the beam energies were within the 1-15 keV range. Once the user defines the type of material that will be studied, CASINO assumes a Gaussian-shaped electron beam, where the user can specify the electron-beam diameter of the instrument. The physical models behind CASINO give information about the absorbed energy in the sample and the electrons escaping the surface of the sample with energy higher than 50 eV (Drouin & Couture, 2007). From such information, different representations of the data, depending on users’ requirements, can be generated by the program. For example, Figure 6 depicts an example of the overview distribution panel display for a thin 35 nm silicon film simulated using 200,000 electrons of 1 keV.

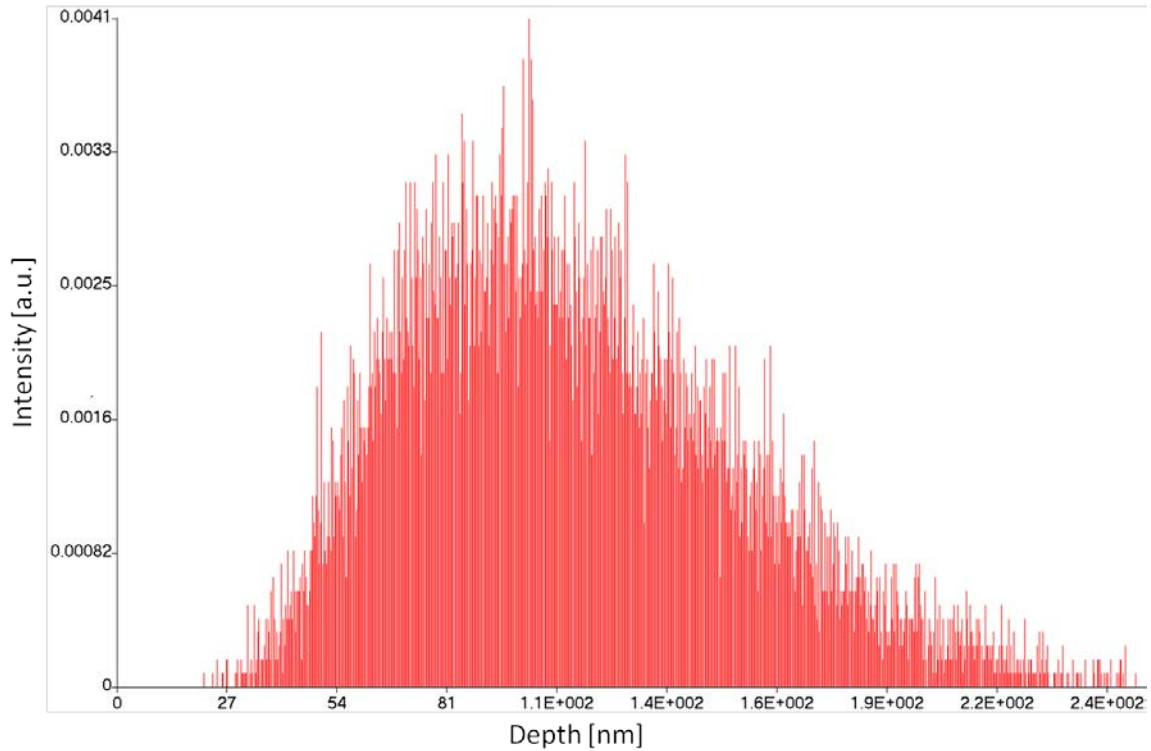


**Figure 6. Different distributions of CASINO output of Z Max for silicon.**

Figure 6 shows the maximum electron beam penetration depth in the silicon sample. As the simulation for  $\text{ThO}_2$  is conducted, the output images should appear different from Figure 6 because there is a vast difference in the atomic number between the silicon example and thorium. Silicon has an atomic number of 14, whereas thorium has an atomic number of 90. Since the depth penetration is dependent on the atomic number, the energy depositions will occur at much shallower depths. The  $\text{ThO}_2$  distributions will be presented in the subsequent chapter.

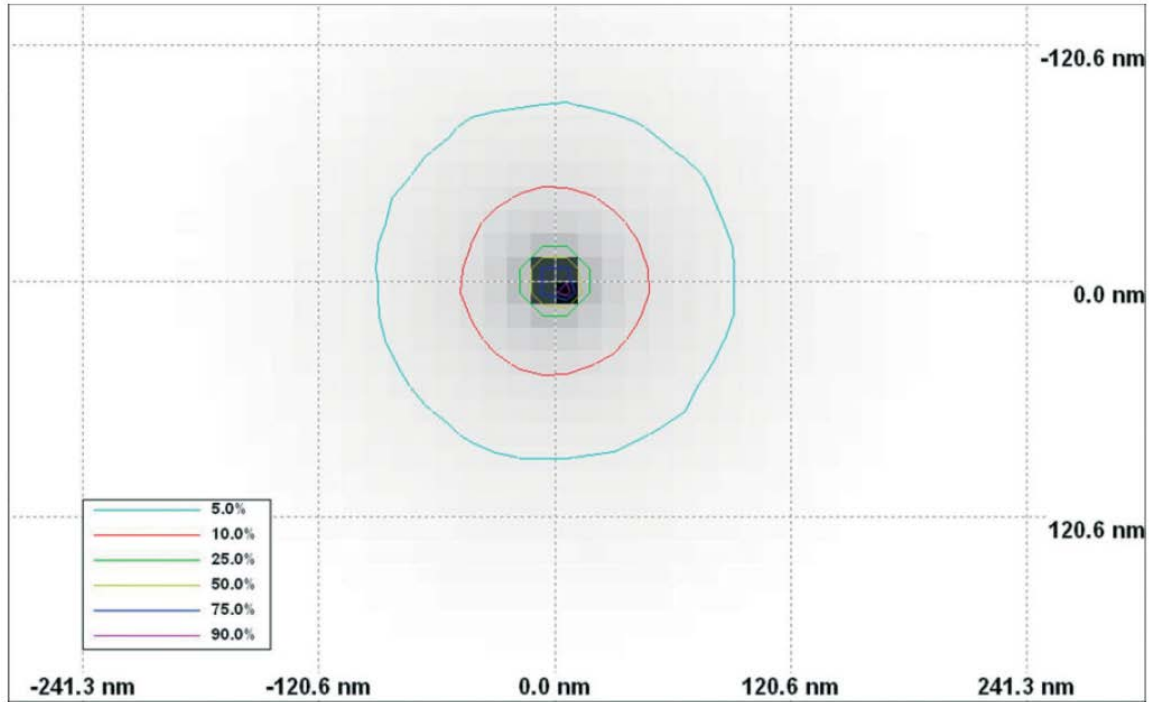


**Figure 7. A CASINO simulation of an arbitrary number of electrons with a random beam energy on an arbitrary sample to show the percentage of the incident energy absorbed on the sample area.**

As the CL occurs, the energy by position feature of CASINO is a very interesting tool to investigate absorbed energy in the sample (Drouin & Couture, 2007). This feature records the amount of energy lost by all the simulated electron trajectories. In Figure 7, the 10% line contains an area, where 90% of the absorbed energy is deposited. A gray shading overlay of the density of absorbed energy is also shown in Figure 7. The gray shade ranges from light to dark as the density increases (Drouin, 2007).

The region of the crystal that interacts with the electron beam is called the excitation volume, and the distance the beam travels is called the penetration depth or electron range,  $R_e$  (Fox, 2010). The penetration depth increases with increasing primary electron energy, and the values of  $R_e$  are in the range of 95-320 nm. The  $R_e$  can be less than 150 nm for electron beam energies below approximately 7 keV. Irradiation by an

electron beam generates electron hole pairs (EHPs) in the excitation volume. The penetration depth can be determined with

$$R_e (\mu m) = \left( \frac{2.76x^{-2}A}{\rho Z^{.889}} \right) E^{1.67}, \quad (2)$$

where  $x$  is the thickness of  $\text{ThO}_2$ ,  $A$  is the atomic weight in g/mol,  $\rho$  is the density in  $\text{g/cm}^3$ ,  $Z$  is the atomic number, and  $E$  is the acceleration voltage in keV (Yoshikawa, 2002). A primary energetic beam experiences energy loss when it interacts with materials. For example, during the irradiation of Si by primary electrons, the electrons suffer energy losses due to the excitation of the valence-band electrons towards the conduction band (Liao, 2012). This inelastic process induces EHP formation. The carriers (holes and electrons) generated inside the interaction volume undergo several processes e.g. escape from the surface, diffuse away from the generation region, undergo recombination, and become partially trapped (Liao, 2012). The number of EHPs generated per incident beam electron, called EHP generation factor, is given by,

$$N^{eh} = (1 - \gamma) \frac{E^p}{E^i} \quad (3)$$

where  $\gamma$  is the fractional electron beam energy loss due to backscattered and emitted electrons,  $E^p$  is the incident beam energy of the primary electron, and  $E^i$  is the ionization energy which is the energy required for the formation of an electron-hole pair (Fox, 2010) (Liao, 2012). The EHPs are produced by a complicated multi-step process involving the re-emission and subsequent inelastic scattering of secondary electrons. For

a wide range of materials, it has been found that  $E^i$  is given by the following simple semi-empirical formula that is related to the band-gap of the materials:

$$E^i = 2.8E_g + E', \quad (4)$$

where  $E'$  depends only on the material, and has a magnitude in the range 0-1 eV (Fox, 2010) and (Liao, 2012). The ionization energy is therefore approximately  $3E_g$ .

By varying the beam energy levels, ThO<sub>2</sub> can be investigated from the surface to bulk states of the material. A higher energy will increase the penetration depth and thereby the volume of excitation, whereas a higher current density will increase the density of excited centers (Lumb, 1978).

## 2.6 Time of Flight Secondary Ion Mass Spectrometry (TOF SIMS)

TOF SIMS is a process where a pulsed primary ion beam bombards the ThO<sub>2</sub> surface with carbon-60 (<sup>60</sup>C or Buckyballs). The pulsed ion beam causes the emission of atomic and molecular secondary ions (Schueler, 1992). The secondary ions are then electrostatically accelerated into a field free drift region with a kinetic energy. Since lighter ions will have higher velocities than the heavier ones, they will arrive at the detector at the end of the drift region earlier than higher masses. Different ion types arrive sequentially at the detector, and they are recorded in the mass spectrum. As the Buckyballs impinge upon ThO<sub>2</sub>, in this measurement the surface is necessarily sputtered and as a result partially cleaned; thereby, exposing more of the true ThO<sub>2</sub> surface.

## 2.7 Atomic Force Microscope (AFM)

In order to confirm that the partial cleaning which occurred in the TOF SIMS measurement was effective, the surfaces of the ThO<sub>2</sub> samples were scanned by an atomic

force microscope (AFM). AFM measured the interatomic forces acting between a detecting tip having a sufficiently sharp point and the surface of ThO<sub>2</sub>. The forces were measured as a displacement of the spring element attached with the detecting tip. Therefore the shape of the ThO<sub>2</sub> surface was charted using a control signal for maintaining the displacement amount of the spring element constant (Yamamoto, 1995). The ThO<sub>2</sub> surface was scanned while maintaining the displacement amount of the spring element at a constant. The image of the ThO<sub>2</sub> surface presented in Chapter 4 was the result of the AFM scanning.

## **2.8 Peak Fit 4.0**

The Peak Fit 4.0 software allowed the broad CL bands to be de-convolved. The minimum number of peaks had to be used in order to resolve features that couple with expected physical processes. In this report, it is evident that five peaks exist to form the broad band peak. Therefore, combinations of the five peaks were set, based-off the first peak at the high energy side, where then the subsequent peaks were off-set by a certain wavelength away from each other. With the increase of temperature, the main broad peak is expected to shift, so a new set-point was set for the first high energy peak and then the subsequent peaks were off-set according to the first fitted combination. After each combinational fit, a regression value was out-putted by Peak Fit 4.0.

## **2.9 Optical Transmittance Measurement**

In addition to the CL experiments, seven optical transmittance measurements were conducted on the ThO<sub>2</sub> crystal samples. A Varian UV-Vis-NIR Spectrophotometer Cary 5000 enabled analysis and characterization of the ThO<sub>2</sub> samples by measuring the



transmittance of ultraviolet and visible radiation. The transmittance spectrum provides information on the wavelengths of electromagnetic radiation that can be transmitted by the ThO<sub>2</sub> crystals. This is determined by varying the wavelength and recording the intensity of the transmitted beam. When photons are absorbed, the energy of the absorbed photons is used to excite a transition between electronic levels (Vij, 1998). The positions of excited states can be obtained from the transmittance spectrum.

## **2.10 Previous Luminescence Studies**

### **2.10.1 Photoluminescence (PL)**

Luminescence can be achieved by exciting the electrons of a substance with high energy electrons or photons. Both CL and Photoluminescence (PL) can effectively determine the electrical properties of ThO<sub>2</sub>. In this previous luminescence study, Harvey and Hallett's research goals were to document well-characterized data on the PL of thoria, to point out that many factors can influence the PL behavior, and to illustrate these behaviors (Harvey, 1976). High purity ThO<sub>2</sub> powder was obtained from the American Potash Chemical Corporation, and they were arc-fused and single crystals were cut from the arc-fused boules with a diamond wire saw (Harvey, 1976). A wide variety of impurities were reported as a result of creating these ThO<sub>2</sub> crystals with the arc-fuse method. The crystals were annealed at 1675 K in four different atmospheres: air, carbon dioxide, carbon monoxide, and dry hydrogen (Harvey, 1976).

The effects of changing the UV excitation wavelength on the PL can be found in Harvey et al. For a pure crystal annealed in air at 1675 K, fast cooled, and measured at 80 K, a broad asymmetric band is observed at 450 nm with 255 nm optimum excitation

(Harvey, 1976). With 280 nm excitation, a sharp line doublet is observed with peaks at 497 and 503 nm. The doublet is attributed to transitions from the  $^3P_0$  and  $^3P_1$  4f levels to the  $^3H_4$  ground state for the trivalent rare earth  $Pr^{+3}$  (Saranathan, 1970). The trivalent rare earth praseodymium was accidentally doped in  $ThO_2$ . Harvey et al concluded that the 450 nm emission is directly dependent on the oxygen vacancy concentration (Harvey, 1976). The same broad asymmetric emission band at “450 nm may be due to closely overlapping F and  $F^+$  centers possibly associated with the reduced state of variable valence impurities (Harvey, 1976).” The origin of the second band at 540 nm is unknown. Lastly, the emission band at 785 nm is probably from the presence of transition metal impurities ( $Fe^{+3}$ ,  $Cr^{+3}$ , or  $Ti^{+2}$ ).

### 2.10.2 Cathodoluminescence (CL)

Vook et al determined the origin and nature of the blue luminescence observed when the surface of a clean thorium crystal is irradiated by an electron beam (2-6 keV) in the presence of various gases. The samples involved in Vook’s experiments consisted of the (533) and (111) faces on high-purity thorium crystals that were mounted onto a thorium substrate of similar purity by spot-welded thorium tabs (Vook & Colmenares, 1982). Then the surfaces were cleaned by argon ion bombardment at 1173 K followed by cooling to room temperature. The CL experiments were conducted at room temperature.

According to Vook, the 468 nm (2.6 eV) main peak is attributed to F center excitation. F centers occur in  $ThO_2$  as a result of oxygen atom vacancies formed during the oxidation process (Colmenares, 1981). Saxena and Pant stated that electron beam irradiation could be expected to excite one of the two trapped electrons in the F center to

the conduction band leaving behind an  $F^+$  center, where only a single electron remains in the oxygen ion vacancy (Saxena, 1954). Vook stated that in the case of very pure  $\text{ThO}_2$  crystals, these electrons drop back down to the  $F^+$  center levels and convert them to excited F centers ( $F^*$ ). The  $F^*$ s lose their energy of excitation by the emission of photons that comprise the large 468 nm band in the CL.

### 2.10.3 Absorption Measurement

Harvey et al examined the effect on the UV absorbance of doping the pure material with selected impurities and conduct related measurements of fluorescence from the pure and doped specimens following both oxidizing and reducing treatments (Harvey & Childs, 1973). Harvey obtained the high-purity  $\text{ThO}_2$  powder from American Potash and Chemical Corp., West Chicago, IL. Batches of  $\text{ThO}_2$  powder were arc-fused, and the sections with parallel sides were cut from the resulting boules using a diamond wire saw. The cut samples were also polished with a series of diamond pastes to produce optically flat single-crystal wafers approximately 0.25 mm thick (Harvey & Childs, 1973). The samples were also put into one of two standard reduction/oxidation conditions by annealing it for one hour at  $1400^\circ\text{C}$  in either high-purity Ar or air (Harvey & Childs, 1973). The absorption spectra from 220 to 370 nm of pure,  $\text{Ca}^{2+}$ -doped, and  $\text{Y}^{3+}$ -doped  $\text{ThO}_2$  crystals can be found in Harvey et al. The doped samples exhibited no obvious bands but exhibited an apparent absorption edge at 240 nm (or 5.16 eV). Harvey et al attribute the absorption bands in the reduced pure material and in both the reduced and the oxidized doped materials to defect centers involving oxygen vacancies (Harvey & Childs, 1973).

### III Experimental Set-Up and Materials Examined

#### 3.1 Chapter Overview

In this chapter, a description of the overall CL system utilized in this study will be given, followed by a description of each component in the system as well as the procedure for obtaining a CL spectrum. Following the system description, the samples studied will be described and shown.

#### 3.2 CL Experimental Set-Up

The CL experiment requires a source of electrons, in this case an electron gun, a sample holder on which to mount the target of  $\text{ThO}_2$ , and an apparatus that facilitates the electron stream to impinge upon the target for a given beam energy and current. As depicted in Figure 8, the experiment apparatus consists of:

- an electron gun with controller
- a cooling system with temperature controller
- a vacuum pumping system
- a spectrometer
- a photomultiplier tube with cooling system
- a means of capturing data & plotting

These components are then mounted in an ultra high vacuum chamber. Images of the lab are depicted in Figure 8, and a schematic of the system is shown in Figure 9.

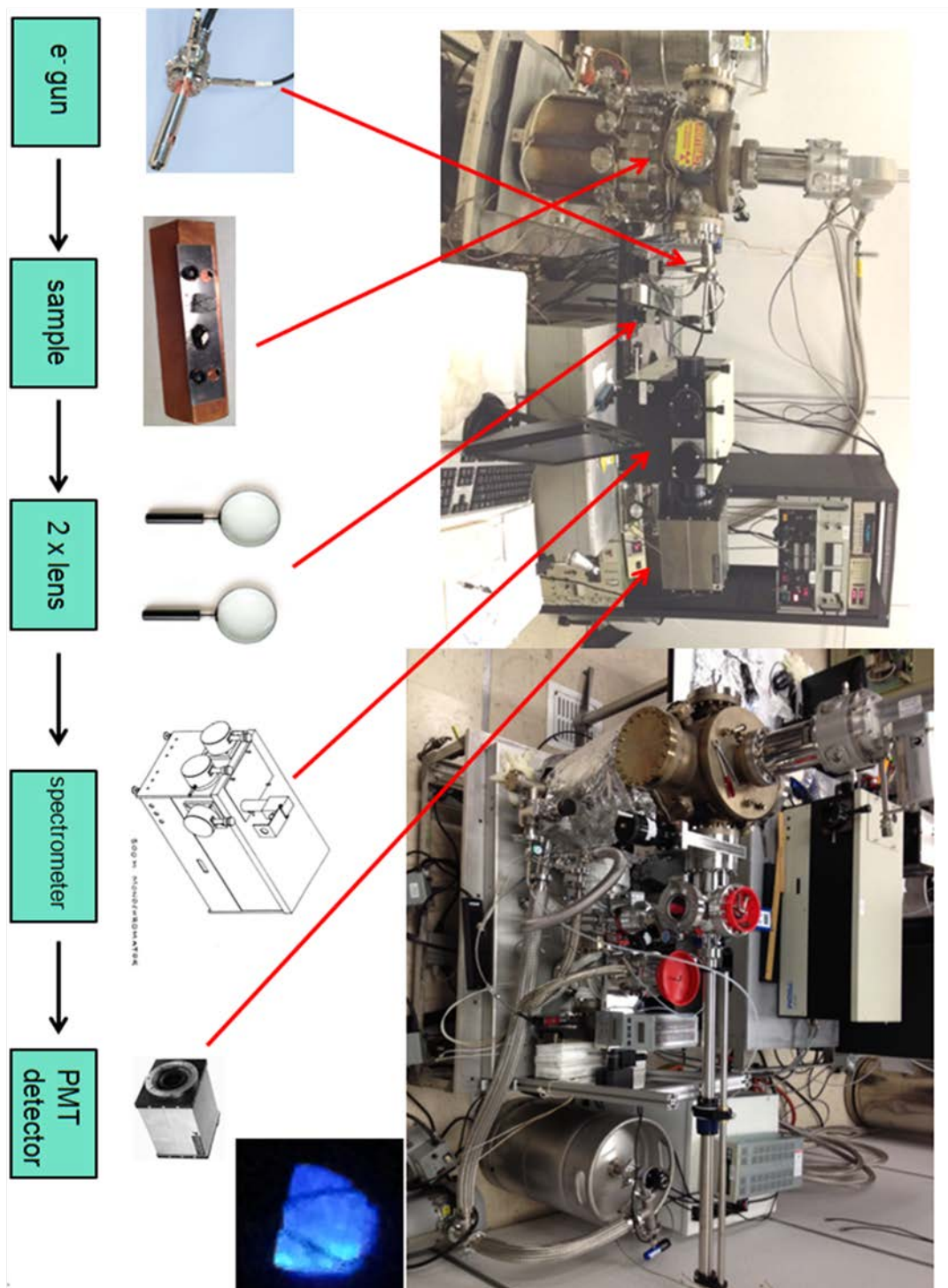
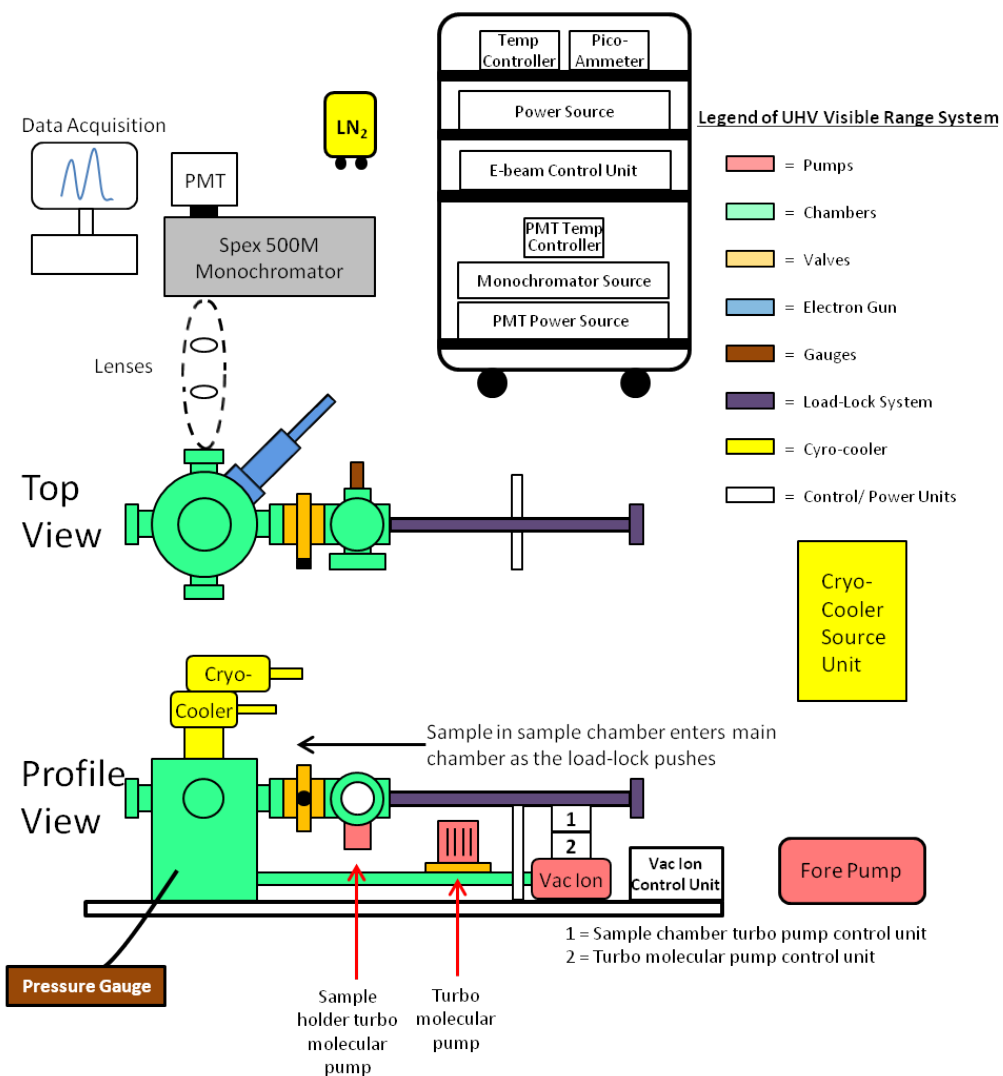


Figure 8. Cathodoluminescence Experimental Set-up.

## AFIT Cathodoluminescence (CL) Experiment



**Figure 9. AFIT CL Experimental Diagram**

**Table 1. Equipment Data for CL Components**

Manufacturer	Component	Serial #	Size [Length x Width x Height in inches]	Specifications
Kimball	EMG-12B	220DZ	22 x 3 x 3	Beam energy 100 eV - 20 keV current 10 nA - 100 $\mu$ A
Leybold	Cryocooler	NE-5302	10.5 x 5 x 21	Cools sample down to 20 K in 90 minutes
Varian	Model 929-7008 Vac-ion pump	649T	14 x 8 x 5	Achieves $1 \times 10^{-7}$ Torr
Agilent	Turbo-molecular pump	IT1211	7 x 5 x 7	Achieves $1 \times 10^{-8}$ Torr
Pfeiffer	Turbo-molecular pump (for sample chamber)	79062008	3.5 x 3.5 x 9	Achieves $2.5 \times 10^{-7}$ Torr
Varian	Dry Scroll pump	50668	15 x 9 x 9	Achieves $7.0 \times 10^{-3}$ Torr
Jobin Yvon--SPEX	500M Spectrometer	6650011420866RH	12 x 22.5 x 13	
Research	PMT Housing	19941-95	10 x 8.5 x 8.5	
SynerJY	Data Acquisition	N/A	N/A	For Windows

Here, the sample is mounted on an oxygen free high conductivity (OFHC)  $^{101}\text{Cu}$  sample holder shown in Figure 10. The samples are fastened onto a thin, highly conductive tantalum sheet as shown in Figure 10 using tantalum wires spot welded to the sheet which is then mounted on the Cu sample holder. The sample is then moved into the main chamber by a horizontal load-lock mechanism which can be seen in Figure 8 and which is depicted in the bottom portion of Figure 9.



**Figure 10.**  $\text{ThO}_2$  and another sample mounted on a thin tantalum sheet by arc welding tantalum wires to secure the samples. The configuration is then secured onto the OFHC  $^{101}\text{Cu}$  sample holder of  $1'' \times 0.375'' \times 0.375''$  (length  $\times$  width  $\times$  height).

The sample load-lock chamber is then pumped down in pressure to  $10^{-6}$  Torr using the sample chamber mini-turbomolecular pump. The main chamber valve is then opened and the sample is moved by the load-lock mechanism. The cold finger is the lower end of the Cryo-cooler that is mounted on top of the main chamber. The cold finger is responsible for cooling the sample down to 20 K. The temperature is monitored and regulated by Lakeshore's temperature controller. The temperature can be lowered or raised to the desired setting for study. From this point on, all the components of the CL apparatus will be described as to how they function. The exact procedure, as to how each CL experiment was conducted, is found in Appendix A.



### 3.2.1 Electron Gun

The electron gun coupled with the spectrometer and the photomultiplier tube detection system allows for a precise and in-depth CL study. The Kimball EMG-12 electron gun shown in Figure 11, has beam energy of 100 eV to 20 keV, and is capable of delivering a beam current of 10 nA to 100  $\mu$ A (Kimball, 1999). The major components of the gun are the cathode, the grid or Wehnelt, the anode, and the deflection plates. The cathode, grid, and anode form a triode of elements.

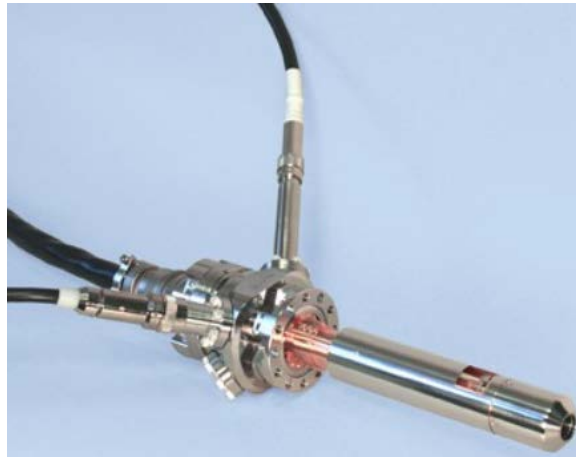


**Figure 11** A derivative of a model EMG-12 electron gun (Kimball Physics, 2012)

The electrons emitted from the cathode are accelerated to full kinetic energy by the triode's electric field, which also causes the beam to crossover in the triode region. This crossover forms the object imaged at the target by the focusing lens.

The cathode is a thermionic emitter that is directly heated by an isolated voltage source. The electron emission is a function of both cathode temperature and energy. The standard cathode uses a refractory metal thermionic emitter consisting of a disk mounted on a hairpin filament wire. The disk provides a circular, planar emission surface that



emits electrons when the filament wire is heated by the voltage source. The cathode is held at a negative high voltage of between 0 and -20 keV.

The Wehnelt or the grid is a tubular structure with an aperture fixed to one end that houses the cathode. The Wehnelt potential is controlled by a voltage source referenced to the negative 0 – 20 kV energy supply, where increasing the Wehnelt potential makes the Wehnelt aperture more negative with respect to the cathode. Therefore, if enough grid potential is applied, the beam will be completely suppressed. The grid is utilized to adjust the beam current without changing the filament source current. These adjustments are extremely critical to the life of the filament.

The anode is an aperture plate that is the third element of the triode, and it is located downstream of the Wehnelt. The trajectory of the electrons emitted from the cathode is determined by the potential difference between the cathode and the anode. An accurate reading of the beam current can be determined by utilizing the Faraday cup assembly that is at the end of the electron gun. During the experiment, the beam power must not exceed two watts.

### **3.2.2 Leybold Coolpower 4.2 GM Cryocooler**

Cryocoolers have recently become the most widely used of the high vacuum cooling systems. This is due to their dry operation and low maintenance requirements (Leybold, 2012). The cryocooler works by cooling internal arrays down to cryogenic temperatures. Figure 12 is a depiction of the equipment that allows the samples used in

this experiment to be held at room temperature down to 20 K. When operating, the cryocooler also serves as a cryopump in addition to its primary role as a sample cooler.



**Figure 12.** COOLPOWER 4.2 GM Cryocooler allows for cooling the samples down to 20 K in approximately 90 minutes. Figure is from (Leybold, 2012).

### 3.2.3 Vacuum System

The vacuum atmosphere required to accomplish the CL measurements consisted of a Varian vac-ion pump, an Agilent turbomolecular pump, a Pfeiffer turbomolecular pump, and a Scroll pump. A steel “beer keg” was used as a buffer volume for the Scroll pump which was used as the roughing pump of the system. Once the main chamber reaches a pressure of  $10^{-2}$  Torr using the Scroll pump, the Agilent turbomolecular pump can be turned-on. This turbo-pump will pump the system down to  $10^{-6}$  Torr. When the main chamber is at  $1.0 \times 10^{-6}$  Torr, the vac-ion pump can be turned-on. The minimum pressure values are required to be reached by each pump; otherwise, the subsequent pump in the system will be over-worked. Once a pressure of  $10^{-6}$  Torr is reached, the vac-ion is always on.

During normal operations involving sample changes utilizing the sample change chamber and load-lock system, the smaller Pfeiffer turbo-pump is utilized. This pump

ensures that the pressure outside the main chamber within the load-lock system is  $10^{-7}$  Torr prior to opening the main chamber to change samples.

### 3.2.4 Spectrometer—Spex 500M

The CL photons emitted from the sample in the evacuated main chamber travel through a quartz window, through two focusing external lenses, and onto the entrance slit of a SPEX 500M spectrometer as shown in Figure 13. These photons are dispersed by the plane grating in the spectrometer and the resulting narrow band of wavelengths passes through the exit slit.

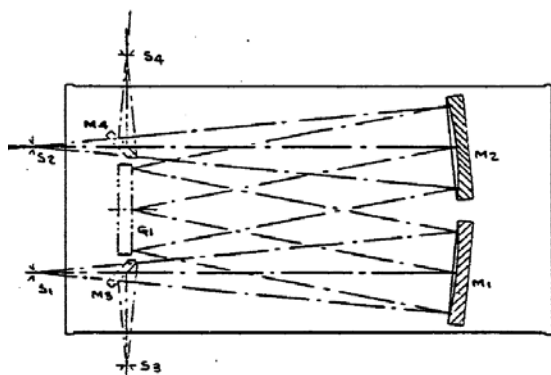


Figure 13. Optical diagram of SPEX 500M monochromator (HORIBA, MSeries).

A scan motor is used to correctly position the grating of the monochromator for the required wavelengths. The grating that is utilized in the spectrometer for these experiments is a holographically recorded 1200 gr/mm grating blazed at  $2500 \text{ \AA}$  with a spectral range of  $1900\text{-}7000 \text{ \AA}$ . After the light leaves the exit slit of the monochromator, it strikes the detector as depicted in Figure 9: PMT.

### 3.2.5 PMT

The PMT creates an electrical current proportional to the number of photons striking the light-sensitive cathode of the PMT (photoemission) (Bennett & Gupta, 2001).



**Figure 14. PMT Housing that contains the actual detector and allows for the detector to be cooled with LN<sub>2</sub> (Research).**

The electrical current coming out of the PMT is amplified by a low-noise current amplifier that provides low bandpass filtering for high-frequency noise reduction, signal amplification, and selectable current-to-voltage conversion ranging from 1 pA/V to 1 mA/V. The electrical noise is further reduced by cooling the PMT housing unit with liquid nitrogen as seen in Figure 14. Cooling of the photocathode of the PMT is required to reduce the thermionic emission from the photocathode and as a result reduce the noise due to the dark current.

### 3.2.6 Data Acquisition—SynerJY

HORIBA Scientific SynerJY™ software is a fully integrated data acquisition and data analysis software for spectroscopic systems. The software provides intuitive control of spectrometers, detectors (offering simultaneous detector control), and accessories. The user-friendly interface allows for quick access to powerful data processing and

presentation tools (HORIBA, SynerJY). SynerJY allows for easy experimentation because its input parameters are user-friendly. The wavelength start and stop positions, the bin size, and the integration time can be easily set for the spectrometer to deliver the data to the PMT detector. SynerJY also provides a tool, where one can stay on a wavelength to determine if there is a signal and then observe as the optimal signal-to-noise ratio is achieved. The maximum signal-to-noise ratio is achieved by:

- Manipulating the two lenses that are positioned between the main chamber of the CL system and the spectrometer in the X-, Y-, and Z-directions
- Manipulating the X- and Y- deflections of the electron beam on the sample target
- Manipulating the beam spot size by varying the focus voltage of the gun
- Increasing the spectrometer entrance and exit slit size widths
- Increasing the beam current
- Cooling the PMT

### **3.3 ThO<sub>2</sub> sample investigated**

Two hydrothermally produced ThO<sub>2</sub> crystals—samples #001TO and #004TO—were studied in this research. Figure 15 presents what sample #001TO looked like prior to and during irradiation.

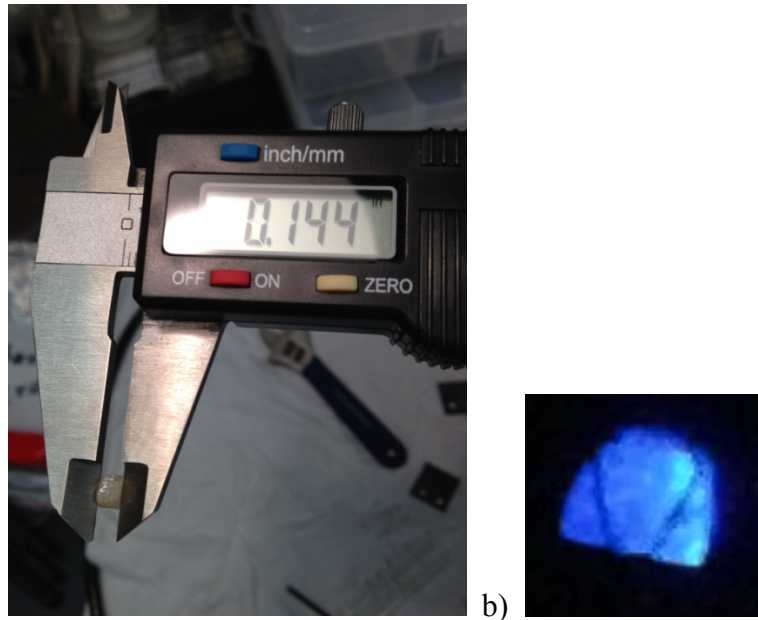


Figure 15.  $\text{ThO}_2$  Sample #001TO a) has a thickness of 0.144 inch, and it b) glows bright blue when it is irradiated with a 10 keV energy and 40  $\mu\text{A}$  beam current.

Sample #001TO has a mass of 0.4199 grams with a thorium weight percent of 2.24%; therefore, 9.4 milligrams of it is thorium. Sample #004TO is a cut and polished sample that is 0.037 grams as depicted in Figure 16.

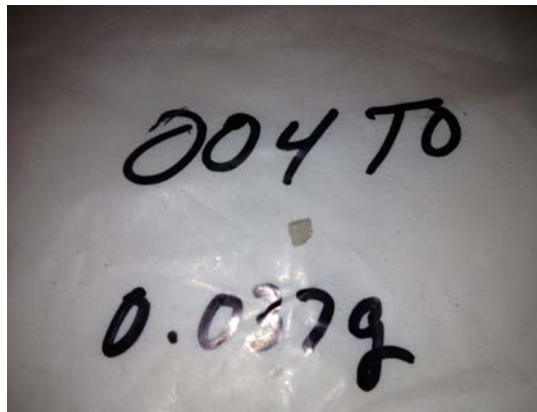


Figure 16. Polished  $\text{ThO}_2$  Sample #004TO.

Depth-resolved CL and optical transmittance measurements were carried out on these two samples.

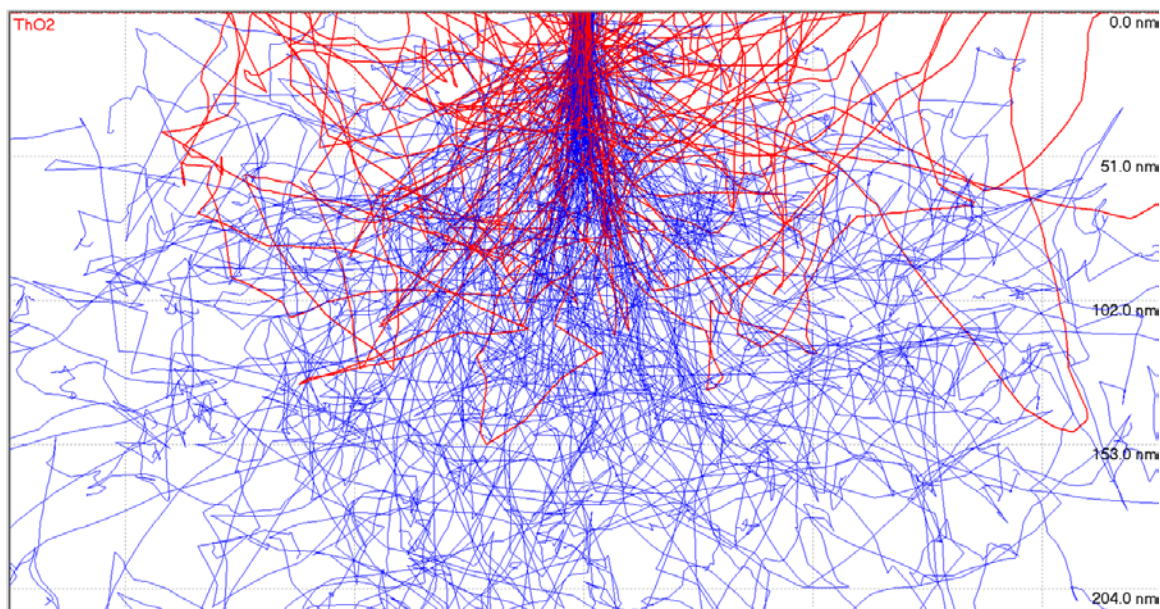
## IV Results and Analysis

### 4.1 Chapter Overview

Based on CASINO simulations of electron beam interactions in ThO<sub>2</sub>, CL measurements were made on the two ThO<sub>2</sub> samples over a range of energies, sample temperatures, and surface conditions. In addition, optical transmittance measurements were also made on both samples. These simulations and measurements are covered in this chapter.

### 4.2 CASINO Depth Penetration Simulation

The purpose of CASINO is to approximate the penetration depth of energetic electrons to be used in depth-resolved CL. The CASINO simulations with 20,000 electrons at various beam energies are presented in Table 2. Backscattered electrons (BEs) are depicted in red, and it is expected that there are so many BEs as a result of the thorium. Figure 17 details how the maximum energy deposition of the blue primary electrons interacts on the surface of ThO<sub>2</sub>, where depths of 95 nm or below are perhaps considered the surface of ThO<sub>2</sub>.



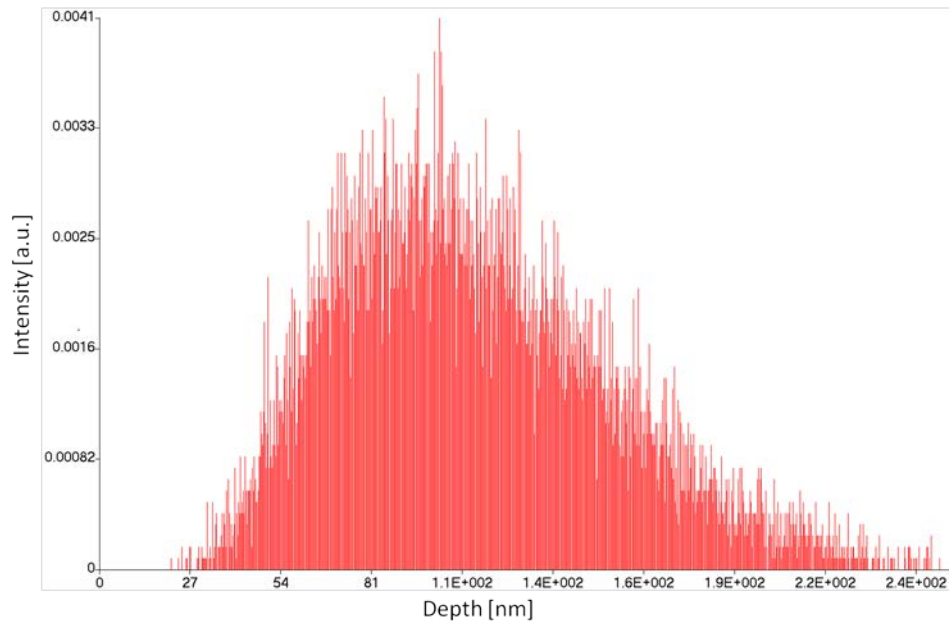
**Figure 17.** CASINO simulation with 20,000 electrons at beam energy of 7 keV interacting on the surface of ThO<sub>2</sub>. Blue is the primary electrons, and red is the backscattered electrons.

Table 2 details how the increase in beam energy results in deeper electron interaction within the bulk of the crystals. According to Mann, the as-grown crystal (Sample #001TO) is more pure because of the hydrothermal growth process. Therefore, it is expected that the spectra from Sample #001TO should be better defined. On the other hand, the cut and polished sample may have unintentional impurities.

**Table 2.** Expected Electron Interaction within ThO<sub>2</sub>.

CASINO Depth Penetration Simulation with 20,000 Electrons	
Beam Energy [keV]	Expected Interaction Depth [nm]
5	95
7	150
10	280
12	320





**Figure 18. ZMax plot of 20,000 electrons of 5 keV energy; maximum energy deposition at approximately 95 nm.**

CASINO simulations depicted in Figure 19 were conducted several times with different beam energies. Maximum energy deposition plots such as the one depicted in Figure 18 were obtained as a result of the CASINO simulations. Table 2 tabulates the maximum energy deposition locations from Figure 18 and other figures for the different beam energies. The location of maximum energy deposition for  $\text{ThO}_2$  when it is excited with 5 keV energy electrons, occurs at approximately 95 nm.

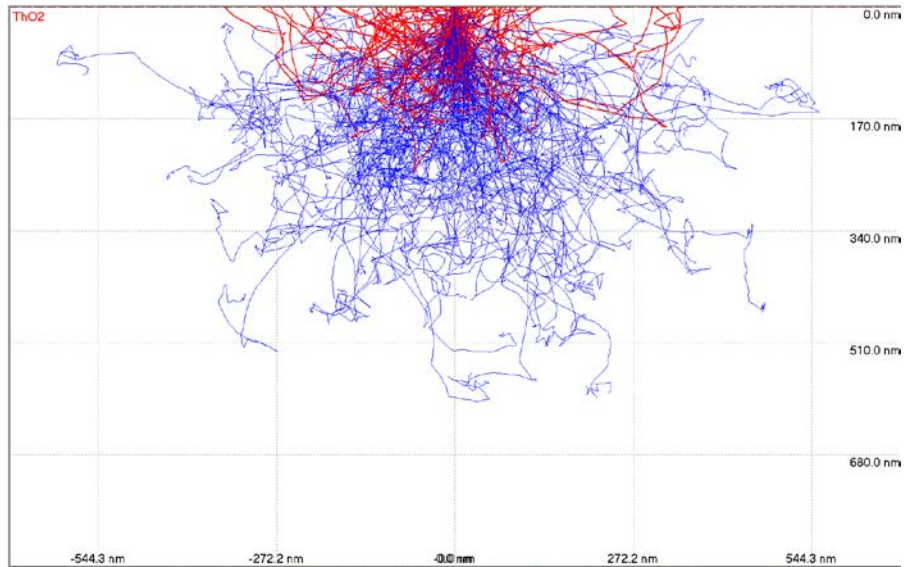


**Figure 19. CASINO simulation with 20,000 electrons at beam energy of 10 keV interacting in the bulk of ThO<sub>2</sub>.**

On the other hand, Figure 19 portrays relatively good electron interaction within the bulk of ThO<sub>2</sub>, and thus what one might expect to find in the actual experiment with a 10 keV beam energy. Here the expected interaction depth is 280 nm. Based on these simulations, the experiment was conducted using beam energies of 5, 7, 10, and 12 keV as well as limited measurements at 1.5 keV to examine the surface of the samples.

### 4.3 ThO<sub>2</sub> Depth-Resolved CL

#### 4.3.1 As-grown Sample #001TO

In this depth-resolved CL experiment, the as-grown and cut and polished samples were examined and compared. The lowest beam energy of 1.5 keV was utilized to begin the study on the as-grown sample. The system response was corrected, but the spectrum in Figure 20 had a significant amount of noise and was not well defined. As the beam energy is increased, the signal-to-noise ratio will become greater resulting in a more defined spectrum. Observe that the main peak location is at 3700 Å at this temperature of 22 K and beam energy of 1.51 keV.

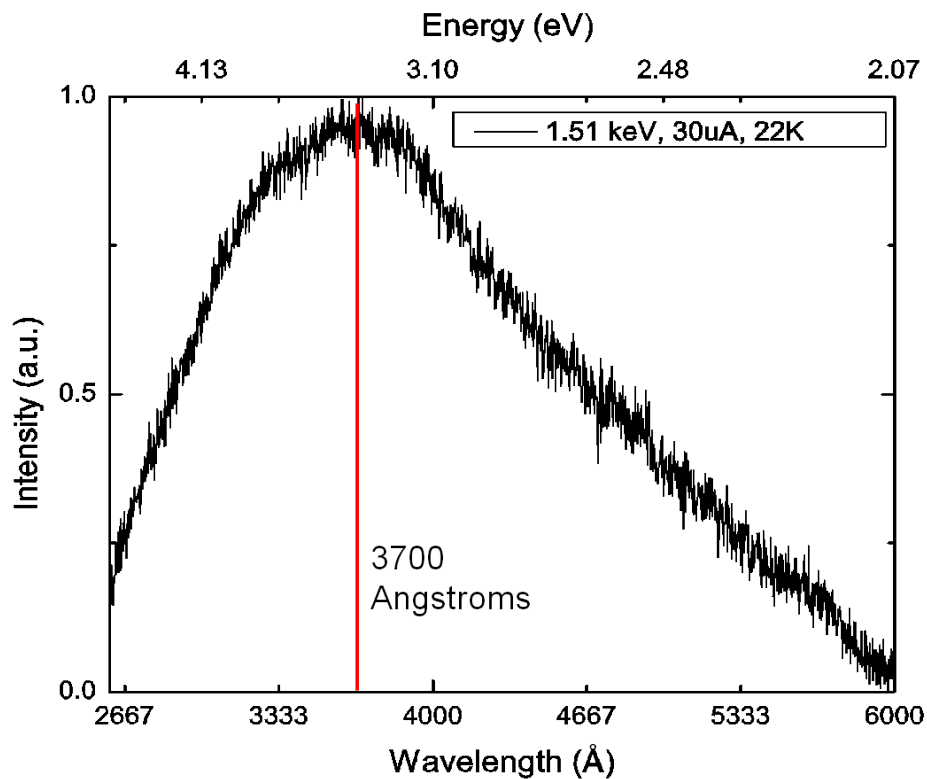


Figure 20. ThO<sub>2</sub> #001TO irradiated with beam energy and current of 1.51 keV and 30 uA, respectively, at 22 K.

As the beam energy was increased from 1.51 keV to the higher energies of 7, 10, and 12 keV, the as-grown ThO<sub>2</sub> sample behaved as shown in Figure 21.

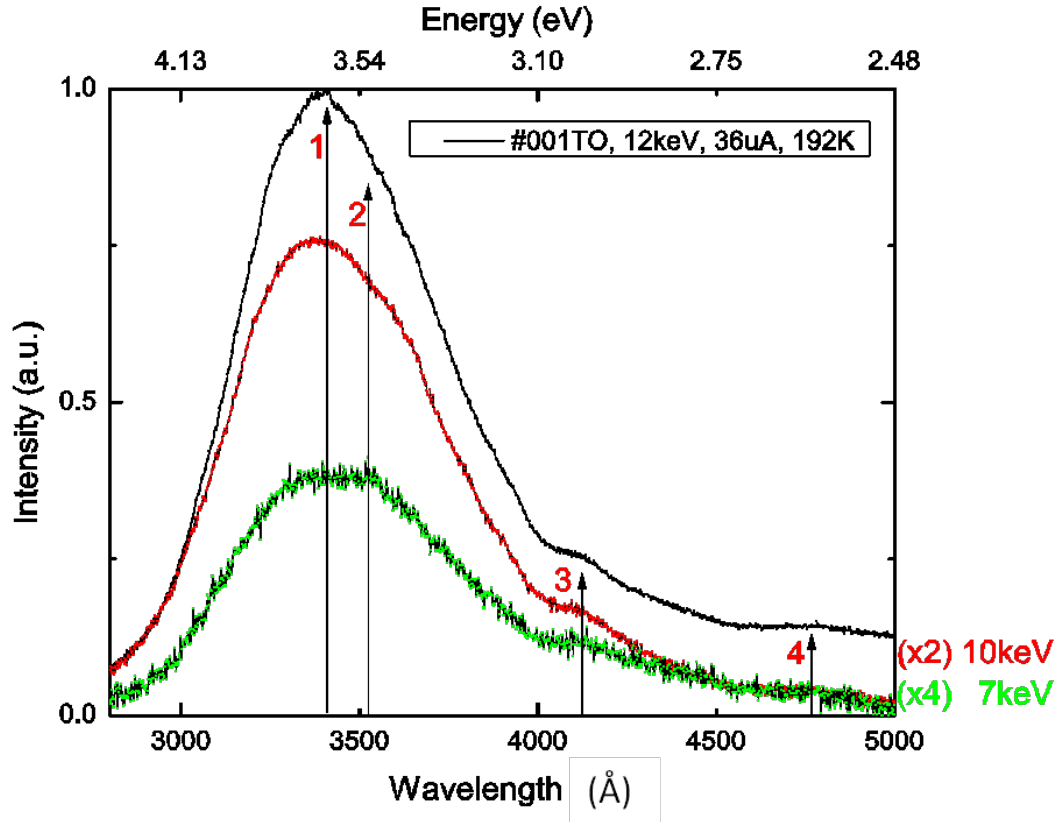


Figure 21. ThO<sub>2</sub> #001TO Energy Dependent Experiment at 192 K.

Table 3. Sample #001TO Energy Dependent Peak Locations at 192 K.

Sample #001TO Energy Dependent Peak Locations: T = 192 K		
Beam Energy [keV]	Location [Å]	Energy [eV]
12	3406	3.639
10	3390	3.656
7	(1) 3396	3.649
	(2) 3518	3.523
Shoulder #1	(3) 4142	2.992
Shoulder #2	(4) 4768	2.599

In Figure 21, varying the beam energy at 192 K yields a set of spectra with the primary peak energy at 3.6 eV (Peak #1). The four peaks tabulated in Table 3 are based off the 7 keV spectrum, and graphically, they correspond well with the 10 and 12 keV

peak locations. The 7 keV spectrum depicts a peak transition from Peak #1 (3396 Å) to Peak #2 (3518 Å). The two shoulders are evident at Peak #3 and Peak #4, which constitute the broad blue luminescence band that can be seen. The as-grown ThO<sub>2</sub> sample appears to have an energy dependency as the peaks shifted as a function of increasing beam energy.

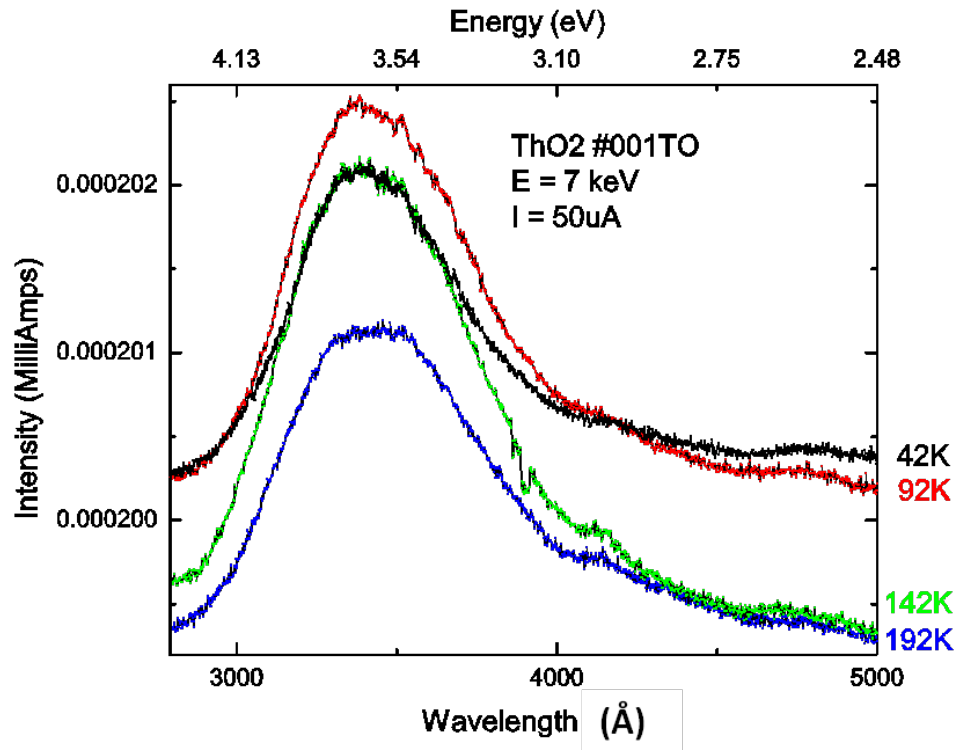


Figure 22. At various temperatures, #001TO irradiated with a beam energy and current of 7 keV and 50 uA, respectively.

Table 4. Sample #001TO Temperature Dependent Peak Locations at 7 keV.

Sample #001TO Temperature Dependent Peak Locations: 7keV, 50uA		
Temperature [°K]	Location [Å]	Energy [eV]
42	3414	3.63
92	3388	3.658
142	3384	3.662
192	3396	3.649
	3518	3.523

A beam energy of 7 keV resulted in peaks identified in Table 4, where the relative intensities decrease and the peaks shift to lower energy levels as a function of increased temperature. The intensities decrease because of the increased phonon-interactions as the temperature is increased. Superimposed peaks create the broad ultraviolet band with an anomalous peak around 4300 Å (2.88 eV) (Gruber & Gray, 1967). At 192 K, the beginning of a double peak transition is observed at 3396 Å and 3518 Å.

Before experimenting in-depth at a beam energy of 10 keV, a single, long run was conducted with an integration time of 1 second per bin to observe if there was any improvement in the definition of the multiple peaks.

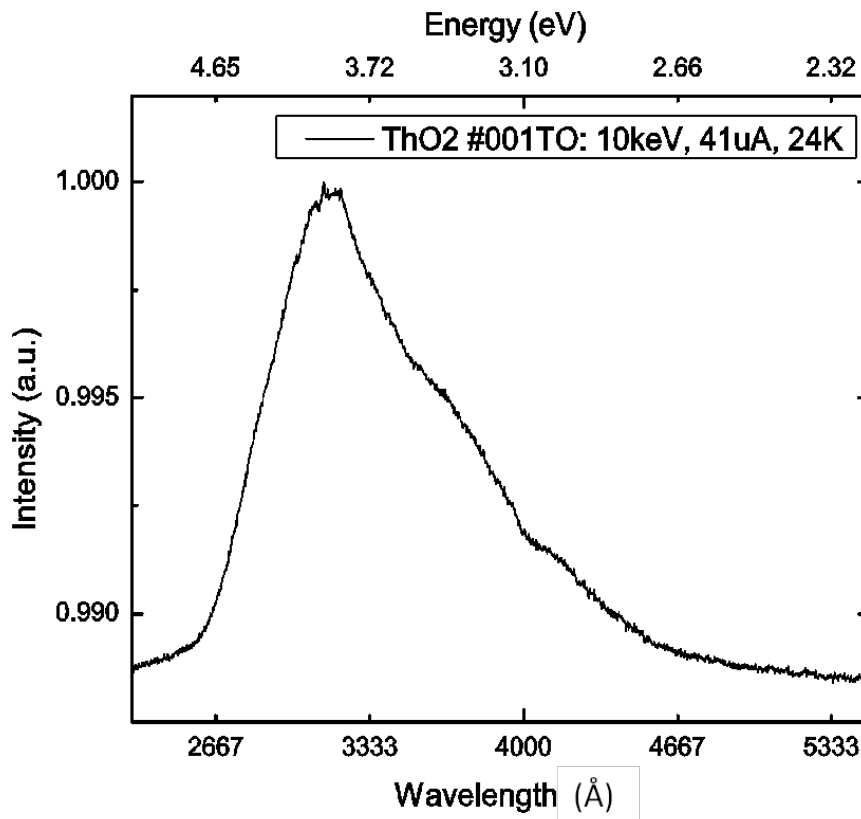


Figure 23. 24 K CL spectrum of ThO2 Sample #001TO obtained using beam energy of 10 keV, beam current of 41 uA, and corrected for system response.

The result is shown in Figure 23 which depicts two distinct shoulders on the lower energy side of the peak. The temperature dependent experiments using a 10 keV beam energy as shown in Figure 24 and Figure 25 further exhibit the locations of these two shoulders (marked by red numbers “2” and “3”) as well as the main peak (red number “1”) and the tail of the broad-band (red number “4”) visible luminescence.

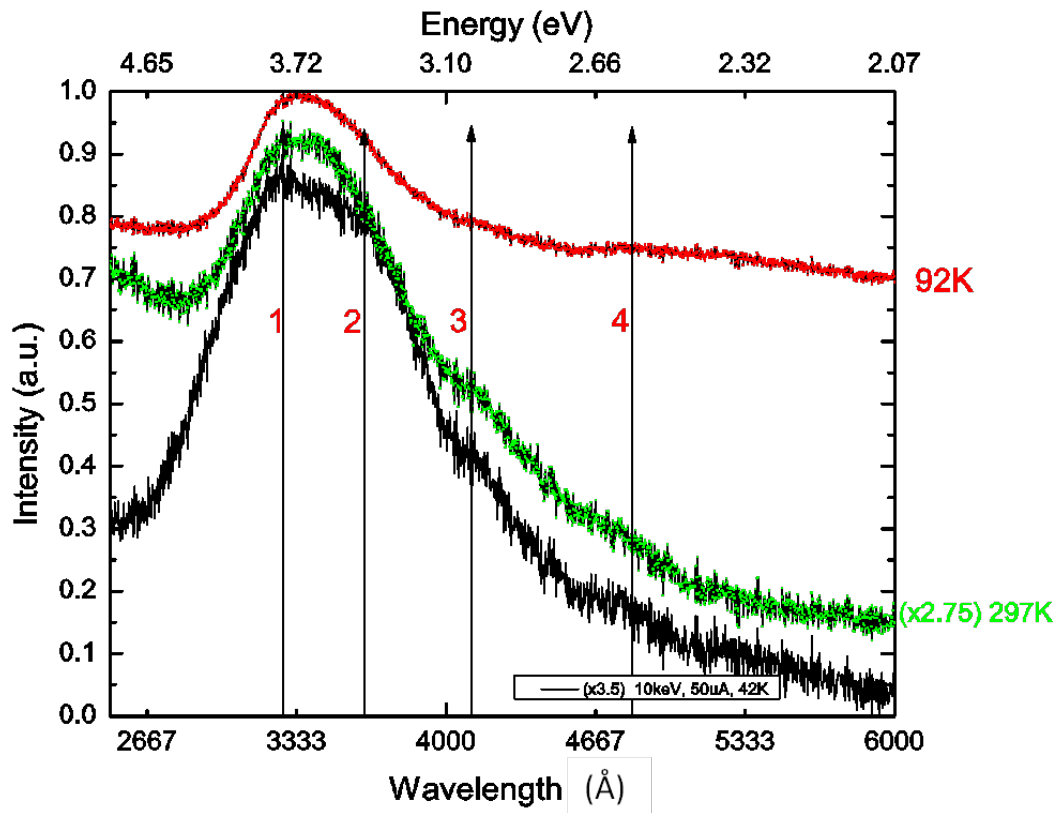


Figure 24. Sample #001TO examined with 10 keV at low and room temperatures

According to Harvey and Hallett, peaks 1 and 2 appear to be competing transitions from the  $^3P_0$  and  $^3P_1$  4f levels to the  $^3H_4$  ground state (Harvey, 1976). The origin of peak 3 is unknown, and peak 4 probably arises from the presence of transition metal impurities such as iron and chromium present in oxidized crystals (Harvey, 1976). Other

researchers like Vook attribute the peaks to F centers in ThO<sub>2</sub> (Vook & Colmenares, 1982).

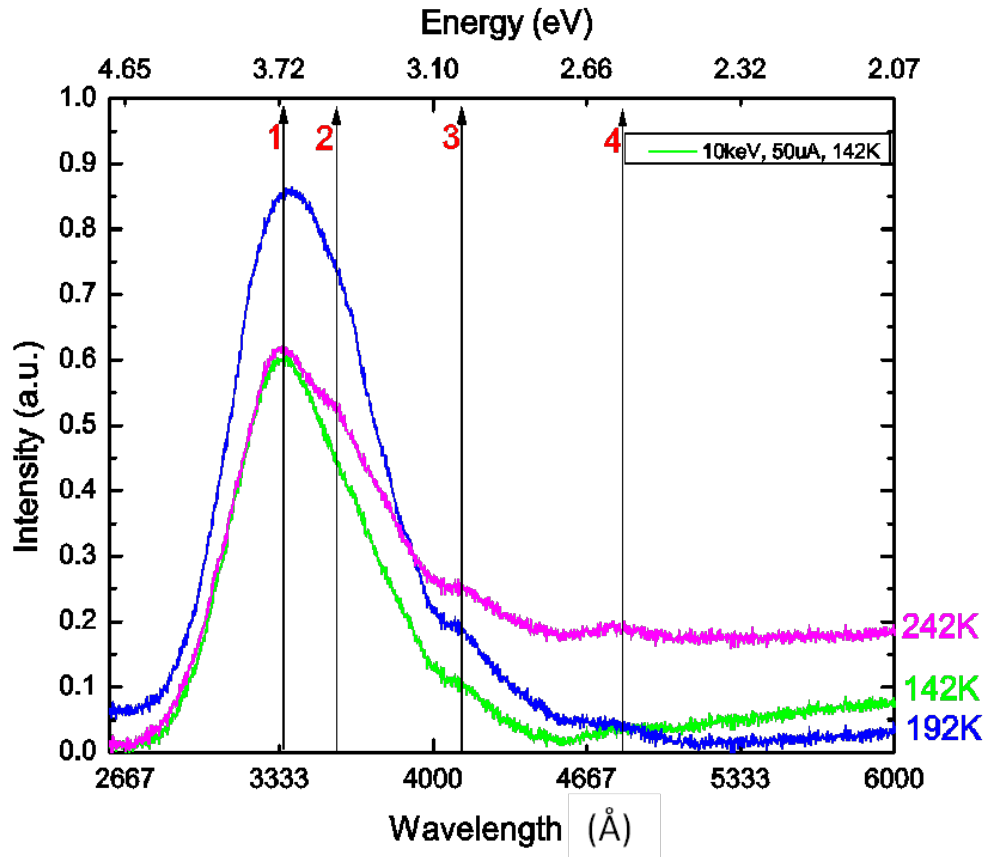


Figure 25. Sample #001TO examined with 10 keV at intermediate temperatures.

Table 5. Sample #001TO Temperature Dependent Peak Locations at 10 keV.

Sample #001TO Temperature Dependent Peak Locations: 10keV, 50uA		
Temperature [°K]	Location [Å]	Energy [eV]
24	3208	3.863
42	3272	3.788
92	3334	3.717
142	3362	3.686
192	3390	3.656
242	(1) 3348	(1) 3.702
	(2) 3562	(2) 3.479
	(3) 4128	(3) 3.002
	(4) 4778	(4) 2.594
297	3390	3.656



The full range of temperatures—24 K through room temperature—allows for a closer investigation of the peak locations and the behavior of ThO<sub>2</sub>'s possible center sites. Based-off Figure 25's 242 K magenta spectrum, the peaks of the two shoulders and the broad-band visible peak were easily identifiable. Table 5 delineates the four peaks for 242 K, and those four peaks remain in their same locations as temperature varies. This is further evidenced in Figure 24 but not as pronounced as in the intermediate temperatures of Figure 25.

Generally, as evidenced by the different temperature variation plots of Figure 24, Figure 25, and Figure 26, it can be claimed that the as-grown ThO<sub>2</sub> sample does not exhibit much temperature dependency.

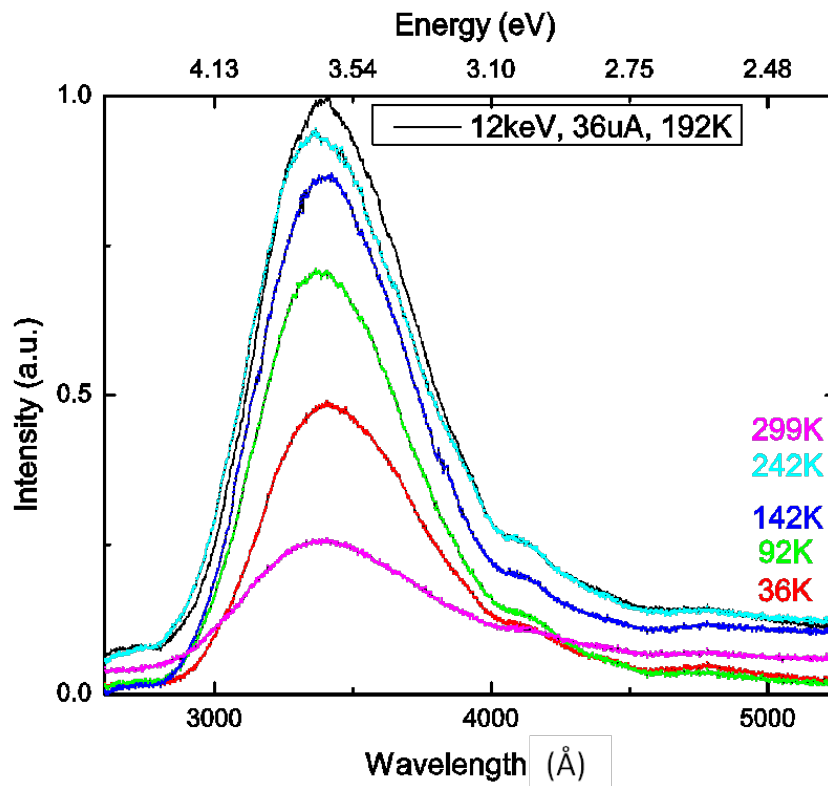


Figure 26. ThO<sub>2</sub> #001TO at various temperatures irradiated by beam energy and current of 12 keV and 36 uA, respectively.

**Table 6. Sample #001TO Temperature Dependent Peak Locations at 12keV.**

Sample #001TO Temperature Dependent Peak Locations: 12keV, 36uA		
Temperature [°K]	Location [Å]	Energy [eV]
36	3406	3.639
92	3366	3.682
142	3426	3.617
192	3406	3.639
242	3366	3.682
299	3410	3.634

The peak locations of the spectra in Figure 26 are tabulated in Table 6. In this case, the electron interactions are now taking place deep within the bulk of ThO<sub>2</sub>. The ripples visible (at the peaks of the 192 K and 242 K spectra) in the broad UV band are possibly due to the microcavity effect (Billeb, Grieshaber, & Stocker, 1997). Changes in the signal intensity in CL depth profiles are caused by variations in physical properties throughout the sample (which can be induced by the electron beam), self-absorption, surface recombination, and recombination competition effects. Although Figure 26 appears uniform and Gaussian, the 92 K and 242 K main peaks tend towards higher energy. This change to higher energy as well as the increase in intensity from 36 K to 242 K can be attributed to recombination competition effects.

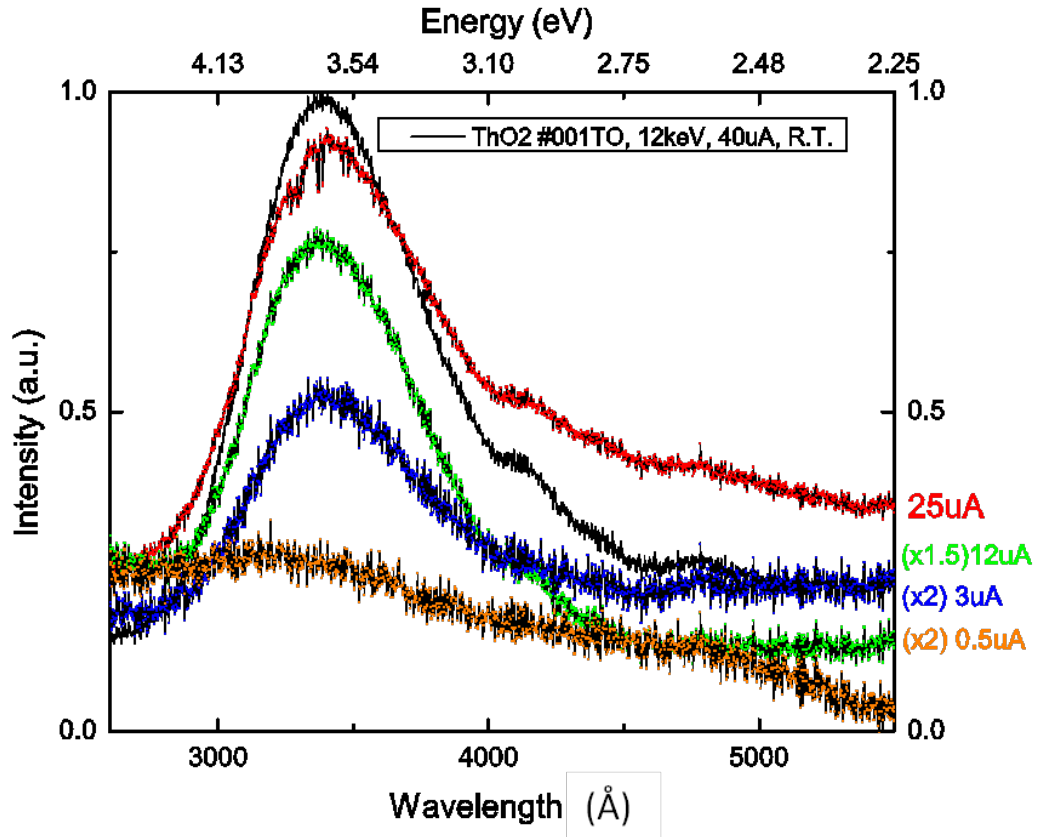


Figure 27. ThO<sub>2</sub> #001TO Current Dependency study at 12 keV.

The variation of the 12 keV spectra with electron beam current is shown in Figure 27. These spectra show a decrease in the electron hole pair recombination with a decrease of the beam current. The spectra generally maintain their form, where the peaks are relatively on the same location. As the current decreases, the shoulders become a broader band.

### 4.3.2 Cut and Polished Sample #004TO

Depth-resolved CL spectra for the polished ThO<sub>2</sub> sample are shown in Figure 28, tabulated in Table 7. These spectra show very little energy dependency.

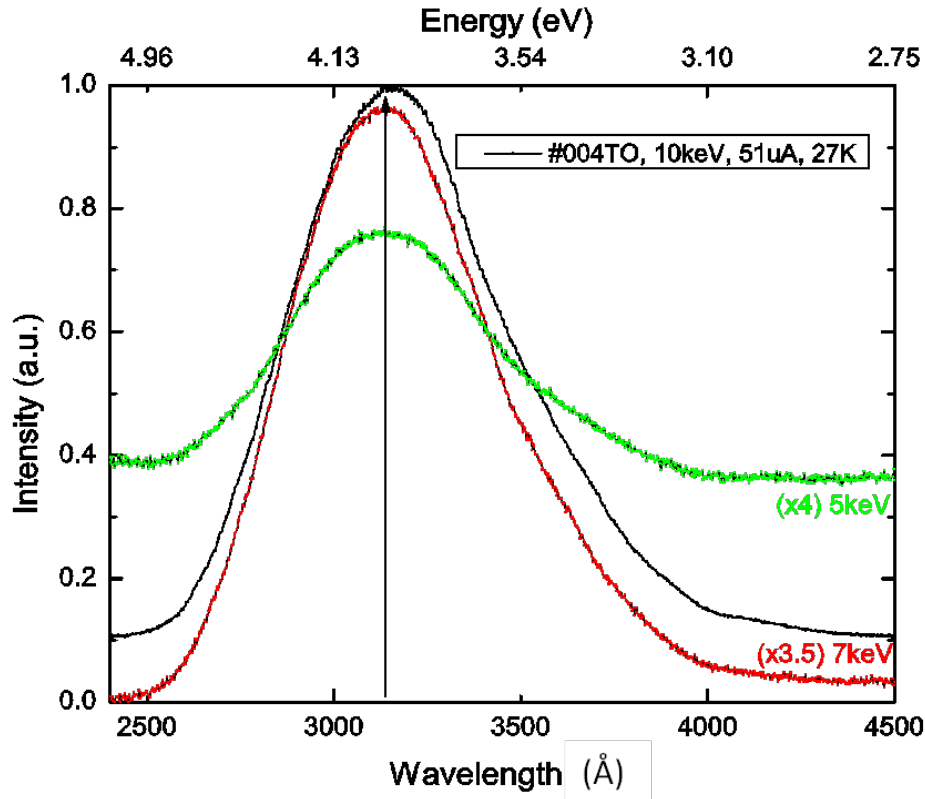


Figure 28. An energy dependency study of ThO<sub>2</sub> #004TO at 27 K.

A uniform shift to shorter wavelengths is observed when the spectra taken at 7 keV and 10 keV beam energies and a temperature of 27 K are compared to the similar spectra taken at 192 K for the as-grown Sample #001TO (Figure 21 and Table 3). In referencing the 192 K Table 3, the peak for the 7 keV beam energy keV is at 3396 Å and the peak for the 10 keV beam energy is at 3390 Å. When the temperature is lowered to

27 K, the polished Sample #004TO has a peak at 3132 Å and 3136 Å for beam energy 7 keV and 10 keV, respectively.

**Table 7. Sample #004TO Energy Dependent Peak Locations at 27 K.**

Sample #004TO Energy Dependent Peak Locations: T = 27 Kelvins		
Beam Energy [keV]	Location [Å]	Energy [eV]
10	3136	3.952
7	3132	3.957
5	3136	3.952

After investigating the energy dependency of the polished ThO<sub>2</sub> sample, a temperature variation study was conducted at beam energies of 5, 7, and 10 keV. Only the 7 keV temperature study will be included in the main body of this report. The other two energy spectra are located in Appendix B.

The set of 7 keV temperature dependent data is depicted in Figure 29 and Figure 30 with the tabulated peak values found in Table 8. Qualitatively, in comparison to the as-grown Sample #001TO's 7 keV runs found in Figure 22, the shape of the polished sample 7 keV spectra are similar to the as-grown spectra. From Table 4, the bottom three values in the table for the as-grown 7 keV have peaks that are close together near 3392 Å. Likewise, from Table 8, the cleaved 7 keV spectra have peaks that are all at 3330 Å. For both samples, the peaks remain stable.

In exploring the temperature dependency for Sample #004TO taken at a beam energy of 7 keV, Figure 29 depicts a sudden shift to a lower energy from the 27 K peak (black line) to the 77 K peak (red line). This sudden shift in energy was investigated in detail by obtaining spectra at 40 K and 52 K to observe that shift. Figure 30 confirms

that the peak does gradually shift to lower energy from 27 K (black), to 40 K (red), to 52 K (green), and then to 77 K (blue).

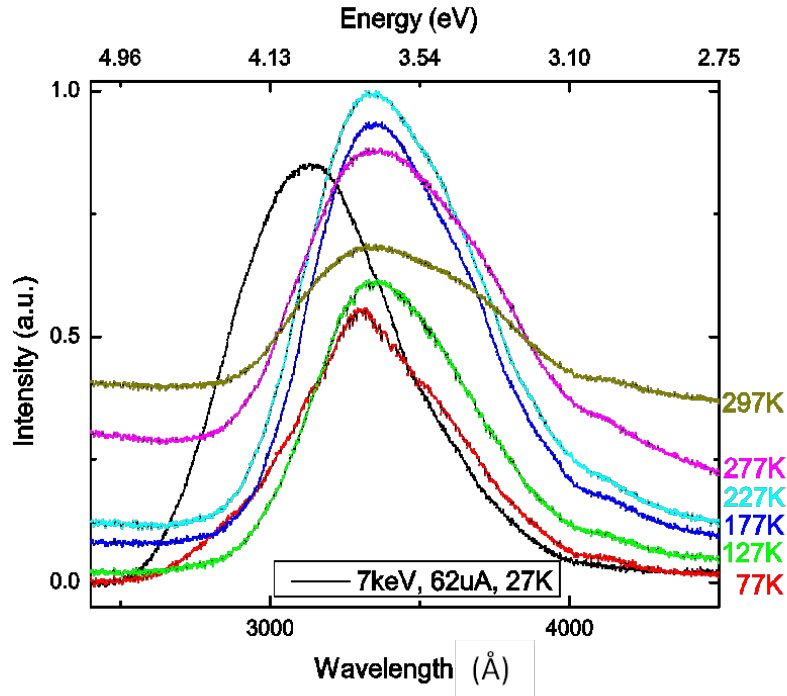


Figure 29. ThO<sub>2</sub> #004TO irradiated with beam energy and current of 7 keV and 62 uA, respectively.

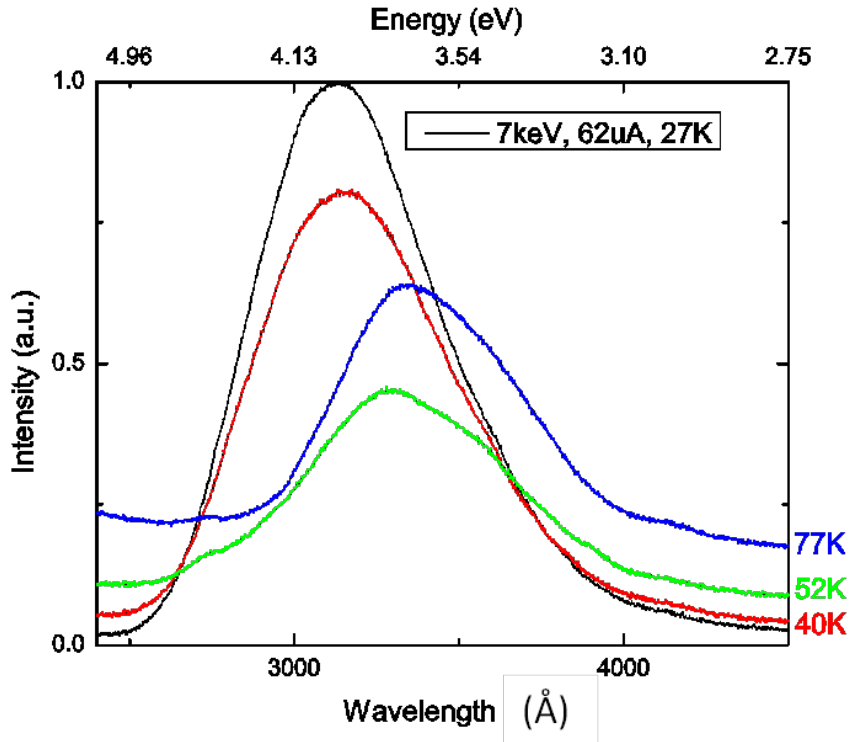


Figure 30. A closer 7 keV inspection of ThO<sub>2</sub> #004TO from 77 K to 40 K to note peak shift.

Table 8. Sample #004TO Temperature Dependent Peak Location at 7 keV.

Sample #004TO Temperature Dependent Peak Locations: 7keV, 62uA		
Temperature [°K]	Location [Å]	Energy [eV]
27	3132	3.957
77	3294	3.762
127	3360	3.689
177	3330	3.722
227	3330	3.722
277	3330	3.722
297	3320	3.733

At this point in the research, the samples were subjected to a TOF-SIMS study by Mr. Tony Kelly. The CL measurements presented from this point on were taken on the samples after the TOF-SIMS measurements. Since the surface was altered as a result of

the TOF-SIMS study, the data that follows will be referred to as post “TOF-SIMS” measurements.



#### 4.4 Post-TOF SIMS Measurements

The as-grown and polished ThO<sub>2</sub> samples were then analyzed by TOF SIMS to determine if any surface artifacts existed as a result of the samples having been exposed to the atmosphere since they were grown over two years ago. TOF-SIMS surface scans for Na and K are shown in Figure 31. Figure 31's red, orange, and yellow spots indicate that sodium (Na), potassium (K), and other elements exist on the surface of the crystals. In TOF-SIMS, the crystal surface was bombarded with Carbon-60 (<sup>60</sup>C) "Buckyballs," which removed six 300 μm<sup>2</sup> spot areas of surface contaminants off the surfaces. As a result of the TOF-SIMS measurements, several surface impurities were identified. These include Na, K, Li, F, H, C, Cs, Cl, CH, C<sub>2</sub>, and OH.

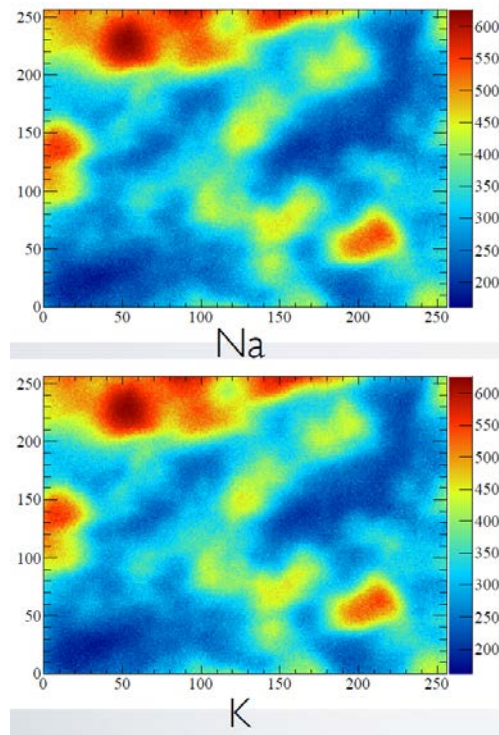
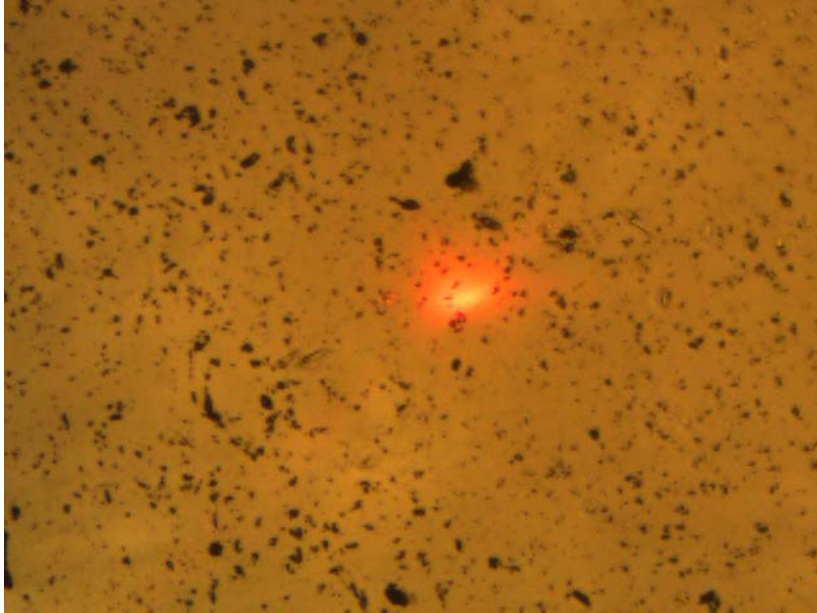


Figure 31. TOF SIMS measurements taken by Mr. Tony Kelly identified Na, K, and other elements present on the surface of the ThO<sub>2</sub> crystals.

In addition to the TOF-SIMS measurements, Atomic Force Microscope (AFM) images were taken of the polished ThO<sub>2</sub> sample. The images also indicated that the surface had been polluted by being exposed to the atmosphere over time. See Figure 32.



**Figure 32. Atomic Force Microscope image of polished ThO<sub>2</sub> was speckled with much surface layer impurities present. Measurement taken by Dr. Alex Li.**

The presence of surface impurities on the samples and the fact that the spots have been “cleaned,” as a result of the “Buckyball” sputtering in TOF SIMS initiated a further in-depth CL investigation of the as-grown and polished samples of “post TOF SIMS” ThO<sub>2</sub>. If enough of the surface has been spot-cleaned, then the expectation is that there should be a change in the radiative behavior of the crystals in CL.

#### 4.4.1 Post-TOF SIMS: CL of As-Grown Sample #001TO

It appears that TOF SIMS partially cleaned the surface of the  $\text{ThO}_2$  crystals, so both the as-grown and cut/polished samples were reinvestigated with depth-resolved CL. First, the as-grown sample had an energy dependency study conducted on it.

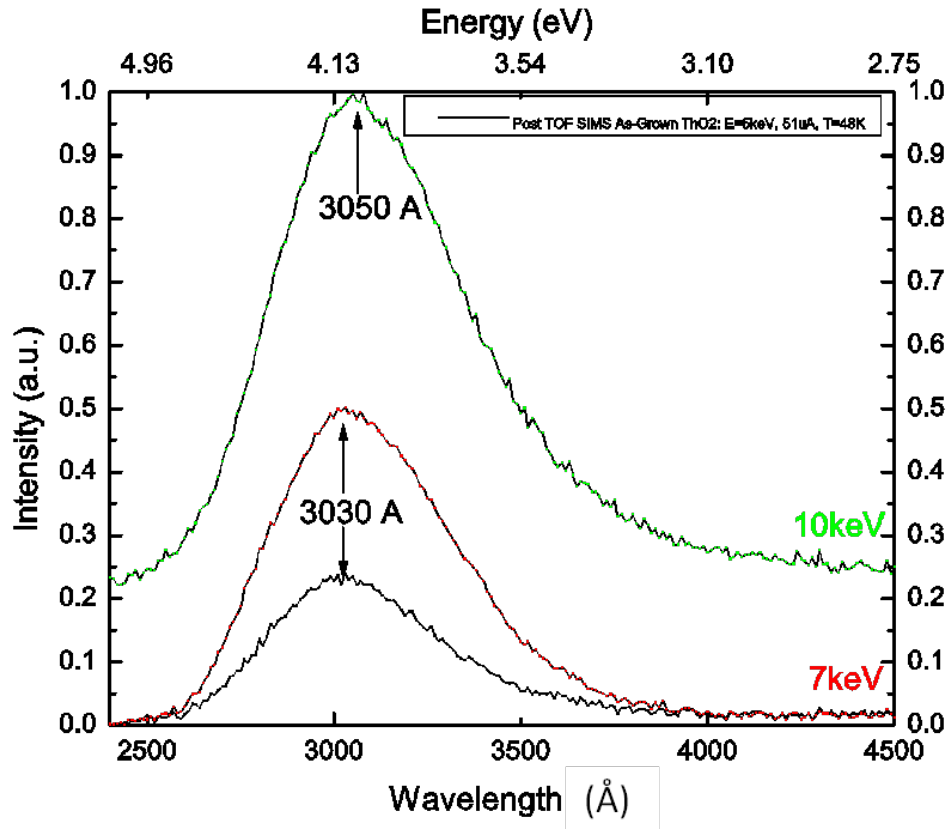


Figure 33. Post-TOF SIMS, As-Grown  $\text{ThO}_2$  Energy Dependency Runs.  $E=5, 7, \& 10$  keV.

**Table 9. Post-TOF SIMS As-Grown ThO<sub>2</sub> Energy Dependent Peak Locations**

Sample #001TO Post-TOF SIMS Energy Dependent Peak Locations		
Beam Energy [keV]	Location [Å]	Energy [eV]
1.51	3012	4.115
	3122	3.970
2.5	3042	4.074
	3126	3.965
5	3030	4.09
7	3030	4.09
10	3050	4.09

The as-grown ThO<sub>2</sub> crystal was irradiated again with varied electron gun energies, which caused photon emission at the energies for the main peaks listed in Table 9. At low beam energies (1.51 and 2.5 keV), the locations of the main peaks did not significantly change, and as the beam energy was increased to 5, 7, and 10 keV, the main peak held constant at approximately 3030 Å. It appears that the Buckyball “cleaning” had an effect on the as-grown sample as the main peak locations now remain relatively stable. This effect, in turn, reverses the trend observed in the pre-TOF SIMS CL measurements, where the peak shifts were highly dependent on the beam energy.

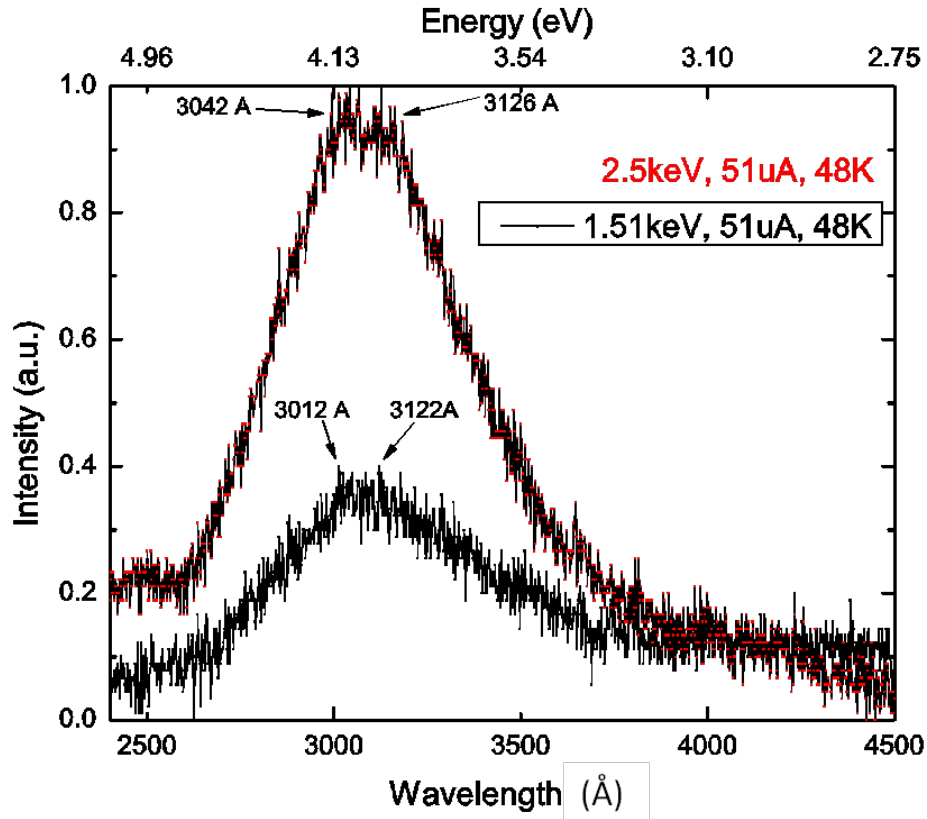


Figure 34. Post-TOF SIMS, As-Grown ThO<sub>2</sub> (#001TO) Energy Dependency Runs. E=1.51 & 2.5 keV.

In contrast to the pre-TOF SIMS CL measurement of this sample in Figure 20, it is observed that there is a more pronounced double peak near 3,000 Å for the 1.51 keV beam energy run in Figure 34. This effect is attributed to the TOF SIMS “cleaning” since more of the true ThO<sub>2</sub> surface is available for the low beam energies to penetrate and interact with the surface. To further confirm that TOF SIMS partially cleaned the ThO<sub>2</sub> samples, the cut/polished sample was further investigated with CL using higher energy electron beams as is shown in Figure 35.

#### 4.4.1 Post-TOF SIMS: CL of Polished Sample #004TO

The first study conducted on the polished sample was an energy dependency study, where the results as shown in Figure 35 are little changed from similar spectra taken before TOF SIMS and furthermore mirror the results of the as-grown post-TOF SIMS energy dependency runs.

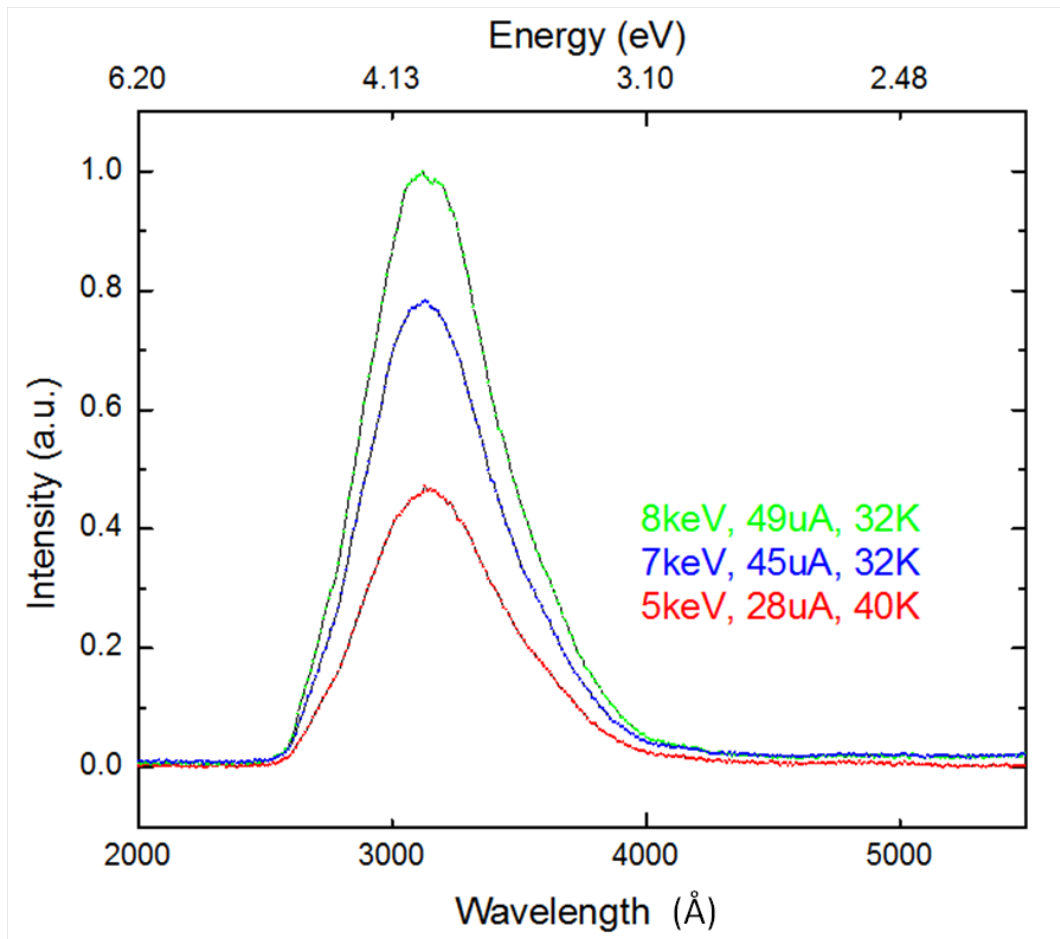


Figure 35. Post-TOF SIMS, Polished  $\text{ThO}_2$  (#004TO) Energy Dependency Runs.

After the energy dependency runs, a deconvolution was conducted on the 1.5 keV spectrum with Peak Fit 4.0 to locate the sub-peaks that comprise the broad UV band.

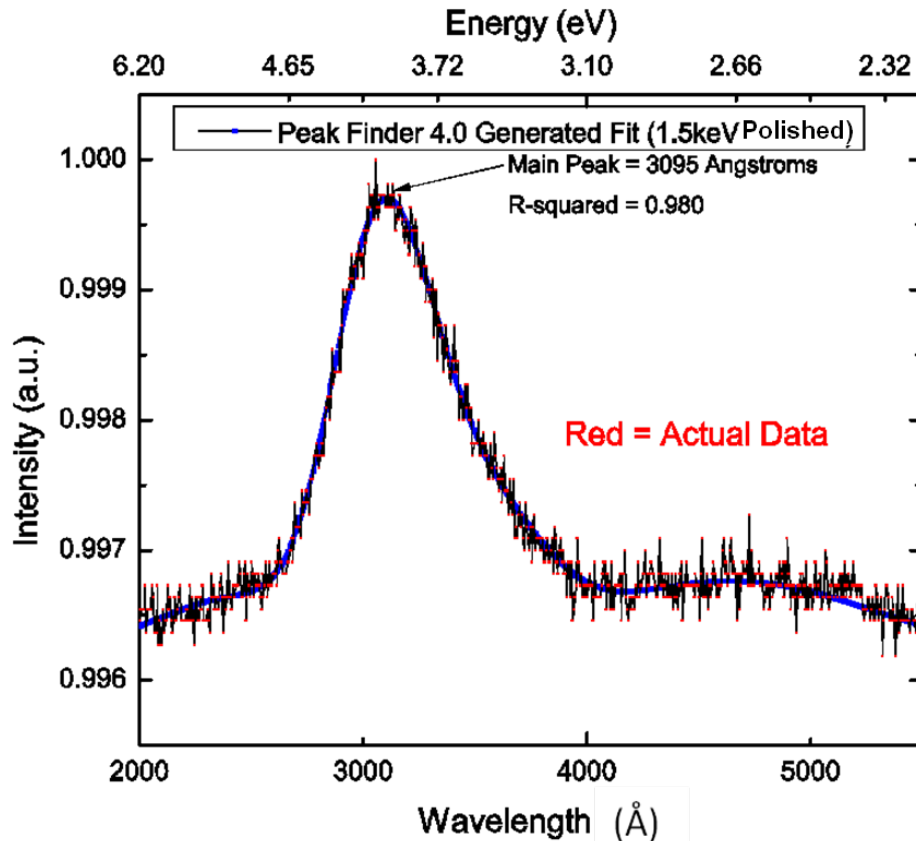


Figure 36. Post-TOF SIMS, Polished ThO<sub>2</sub> irradiated with 1.5 keV beam energy, 51 uA beam current at 48 K (actual data in red). Also portrayed is the peak fit generated spectrum (in blue).

The cut/polished ThO<sub>2</sub> crystal was rigorously investigated again but this time with peak fitting and de-convolving the main peaks to observe whether or not the de-convolved mini-peaks' wavelength differences remain the same (wavelength and energy). These results are shown in Table 10. Table 10 provides the five peak locations as determined from Peak Fit 4.0 for each of the spectra for 1.5, 2.5, and 7 keV. The differences between these peaks are also shown. Observe that the differences in mini-peak locations (or  $\Delta\lambda$ ) are relatively the same for beam energies 1.51 keV and 7 keV. Furthermore, the mini-

peak wavelength differences for the 2.5 keV energy's peaks (2) and (3) are relatively close to those of the other beam energies.



**Table 10. Post-TOF SIMS Polished ThO<sub>2</sub> Sample Energy Dependent Peak Locations, Peak-Fitted De-convolved Peak Locations with Wavelength Differences, and Regression Values. (1)-(5) denote the mini-peaks de-convolved.**

Cleaved Sample #004TO Post-TOF SIMS Energy Dependent Peak Locations				
Beam Energy [keV]	Location [Å]	$\Delta\lambda$ [Å]	Energy [eV]	R <sup>2</sup>
1.5	3095		4.01	0.98
	(1) 2432.1		5.09	
		571.9		
	(2) 3004.0		4.12	
		195.8		
	(3) 3199.8		3.87	
		388.6		
	(4) 3588.4		3.45	
	(5) 4654.5		2.66	
2.5	3100.0		3.99	0.996
	(1) 2440 (x50)		5.08	
		570		
	(2) 3010		4.12	
		190		
	(3) 3200		3.87	
		400		
	(4) 3600		3.44	
	(5) 4670		2.65	
5	3130		3.96	
7	3340		3.71	0.998
	(1) 2724.2		4.55	
		559.6		
	(2) 3283.7		3.77	
		214.5		
	(3) 3498.2		3.54	
		366.8		
	(4) 3865.0		3.20	
	(5) 4946.7		2.50	
8	3110		3.98	

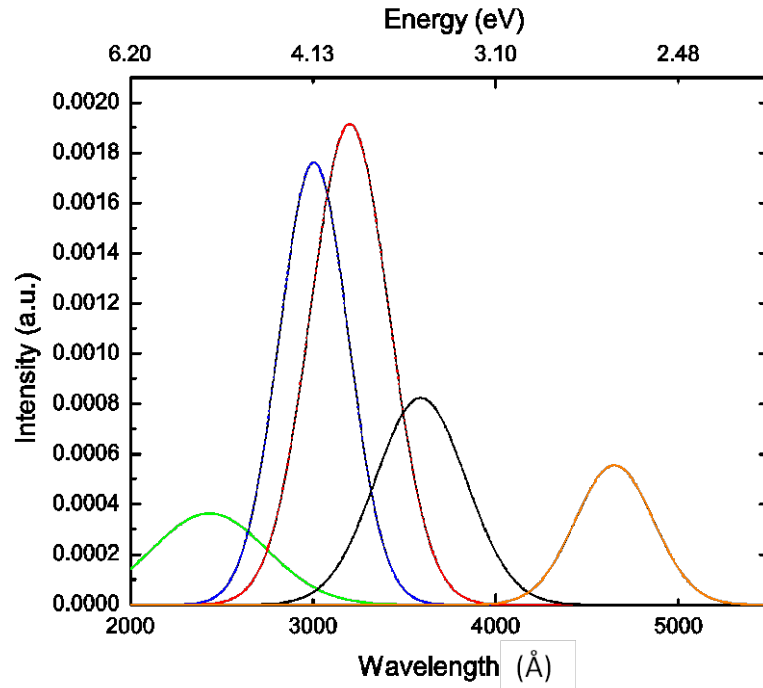


Figure 37. Post-TOF SIMS, Polished ThO<sub>2</sub> de-convolution with 5 superimposed peaks that result in a  $R^2 = 0.980$  generated peak fit depicted in Figure 36.

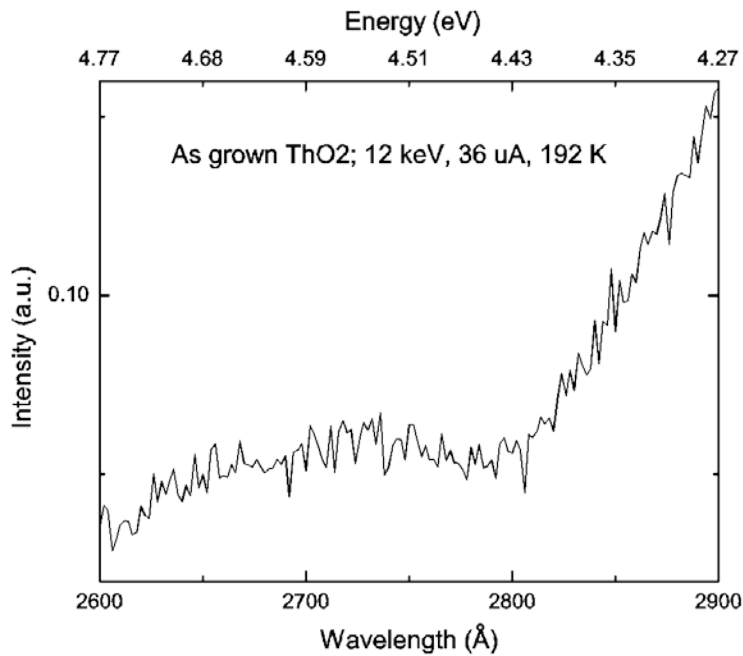


Figure 38. Zoomed-in depiction of the as-grown 12 keV, 192 K spectrum; Figure 26.

Examination of the spectra in Figure 34 indicates the existence of a small peak near 2500 Å. Figure 37 depicts how the addition of the small peak at 2432.1 Å enables the regression  $R^2$  value to be increased 0.980, whereas without the peak the  $R^2$  value is 0.95. This effect combined by the addition of the short wavelength (high energy) peaks on the other beam energy experiments demonstrates an existence of a small peak that is normally dominated by the main UV peak. There are several instances that the small high energy peak actually manifests itself in both the cleaved and as-grown spectra. The manifestations highly indicate the existence of a small peak even more.

In Figure 26, the as-grown 12 keV 192 K (spectrum in black) and the 242 K (teal color spectrum) runs, note that there exists a small peak slightly above 2500 Å that is dwarfed by the prominent UV peak. Figure 38 zoomed-in Figure 26's spectrum (12 keV, 192 K). Observe that there is a peak between 2600 – 2800 Å. Lastly, in Figure 30, as we inspect the drastic shift in peaks due to temperature variance, observe the evidence of a bump in the higher energy side of the 52 K and 77 K spectra.

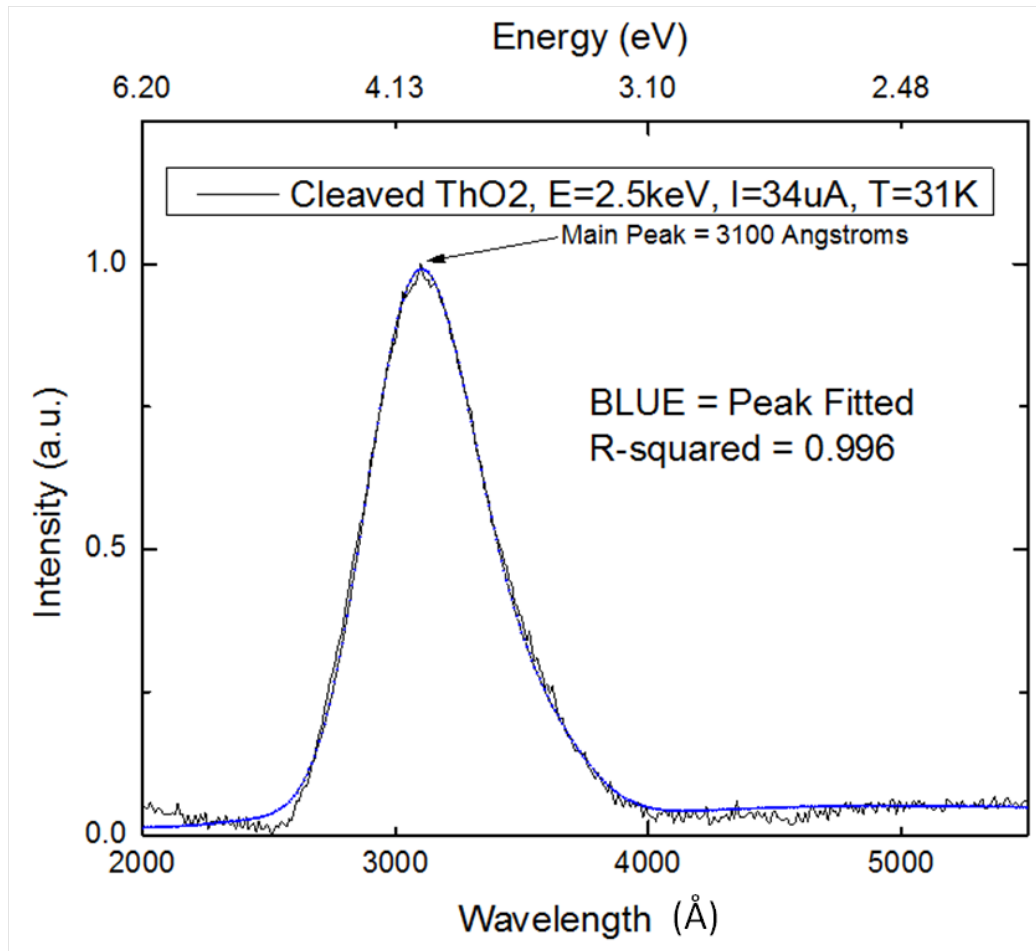


Figure 39. Post-TOF SIMS, Cut/Polished ThO<sub>2</sub> irradiated with 2.5 keV beam energy, 34 uA beam current at 31 K (actual data in black). Peak-fitted spectrum with a R<sup>2</sup>=0.996 (in blue).

The post-TOF SIMS CL measurements with de-convolution further indicate that a peak exists on the higher energy side of the main peak. As a result of TOF SIMS' cleaning, that small peak is more pronounced. The de-convolution analysis indicates that the addition of the—for example, the 2440 Å peak—refines the Peak Fit R<sup>2</sup> value to equal 0.996 in Figure 39.

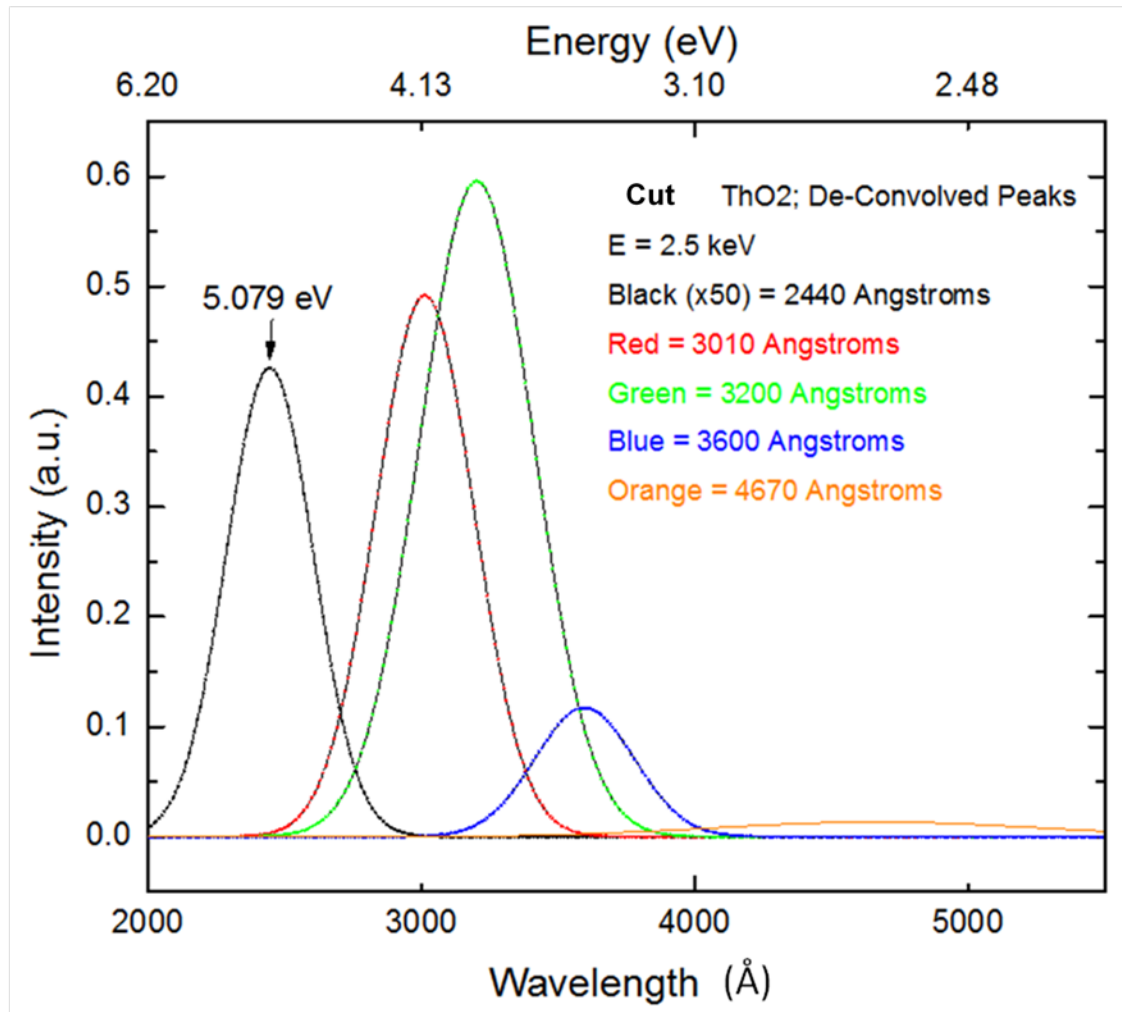


Figure 40. Post-TOF SIMS, Cu and Polished ThO<sub>2</sub> de-convolution with 5 superimposed peaks that result in a  $R^2 = 0.996$  generated peak fit depicted in Figure 39.

The inclusion of a well-fit mini-peak that steadily maintains its mini-peak wavelength difference as the main peak shifts due to either energy or temperature variances while providing an extremely good overall fit highly suggests of a small peak's existence. After deconvolving the 1.5 and 2.5 keV spectra, nine more spectra were deconvolved. As shown in Table 11, spectra from pre- and post-TOF SIMS of both as-grown and polished ThO<sub>2</sub> crystals were deconvolved to show that the highest energy photon peak can be the band gap.

**Table 11. Peak Fit 4.0 Deconvolution of CL Peaks with 5-sub-peaks; the wavelength differences between each combination of fits based-off the shortest wavelength (band gap); and regression value of best-fit.**

Pre-TOF SIMS, As-Grown											
Deconvolution #	Beam Energy[keV] Temperature [K]	R-squared value	Peak 1 [Å]	$\Delta\lambda$ [Å]	Peak 2[Å]	$\Delta\lambda$ [Å]	Peak 3[Å]	$\Delta\lambda$ [Å]	Peak 4[Å]	$\Delta\lambda$ [Å]	Peak 5[Å]
1	1.51 T=22K	0.984	2760.5	573.1	3333.6	193.1	3526.7	389.2	3915.9	1066.6	4982.5
2	7 T=42K	0.988	2760.1	572.6	3332.7	197.1	3529.8	389	3918.8	1063.7	4982.5
3	10 T=24K	0.9955	2539.4	570.9	3110.3	189.2	3299.5	381.8	3681.3	1285.4	4966.7
Pre-TOF SIMS, Cleaved											
4	7 T=52K	0.996	2742.1	573.1	3315.2	193.1	3508.3	389.2	3897.5	*602.5	*4500
5	10 T=127K	0.996	2756.6	577.9	3334.5	194.4	3528.9	391.4	3920.3	1061.3	4981.6
Post-TOF SIMS, As-Grown											
6	1.51 T=48K	0.904	2444.4	569.2	3013.6	177.3	3190.9	411.6	3602.5	*890.9	*4493.4
7	2.5 T=48K	0.97	2444.4	569.2	3013.6	177.3	3190.9	411.6	3602.5	*890.9	*4493.4
8	7 T=46K	0.997	2420.3	564.8	2985.1	201.4	3186.5	387.5	3574	*917.2	*4491.2
Post-TOF SIMS, Cleaved											
9	1.51 T=29K	0.98	2432.1	571.9	3004	195.8	3199.8	388.6	3588.4	1066.1	4654.5
10	2.5 T=31K	0.996	2440	570	3010	190	3200	400	3600	1070	4670
11	7 T=32K	0.998	2508.8	545.5	3054.3	232.9	3287.2	377	3664.2	1072	4736.9
				562.4667 AVG	206.23333 AVG	388.5333 AVG	1097.87 AVG				

The de-convolution analysis of the main peak and the experimental results described in the discussion of previous experimental studies highly indicate that the peak at 2500 Å is associated with the band gap. Thus from the depth-resolved CL results, one can conjecture that the hydrothermally grown ThO<sub>2</sub>'s absorption edge is 5.1 eV (2436 Å). The value of 5.1 eV is based on the Peak #1 average of Deconvolution #6-10 in Table 11.

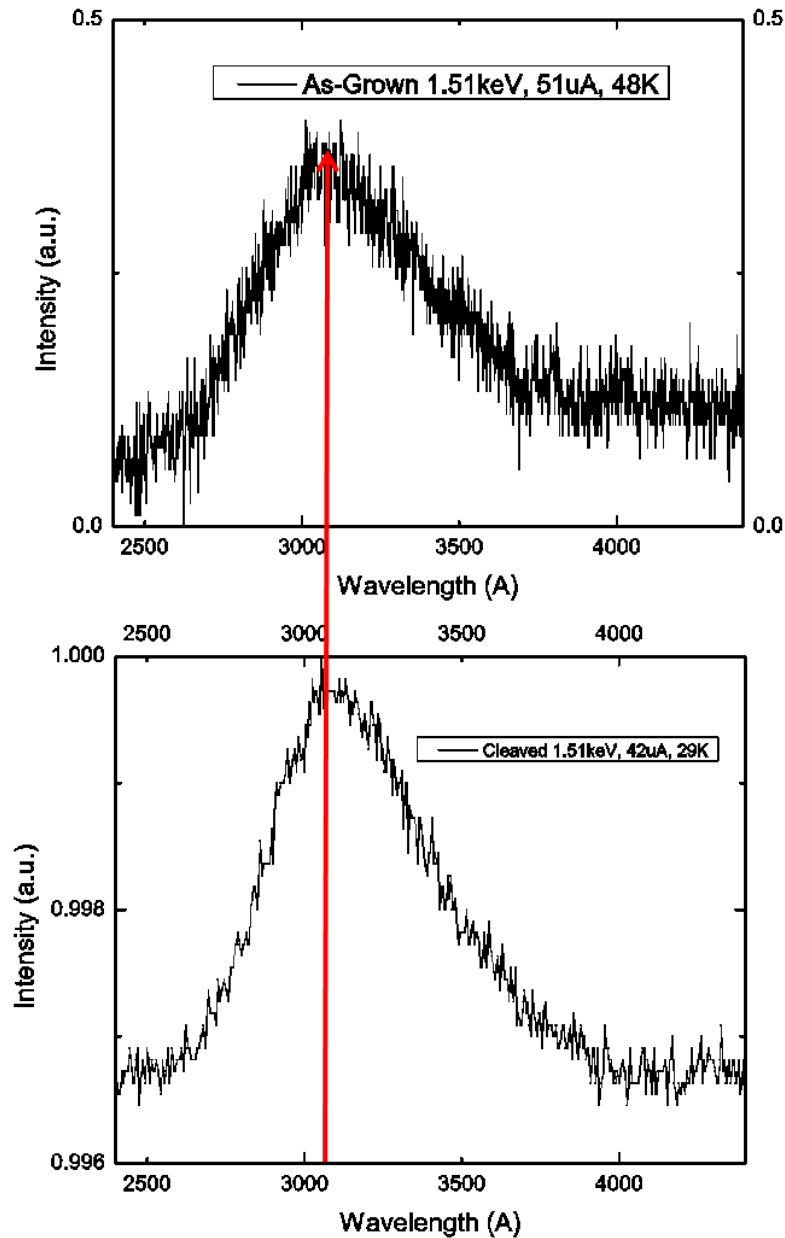


**Figure 41. Post-TOF SIMS ThO<sub>2</sub> Comparison between As-Grown and Polished samples; both irradiated at beam energy of 1.51 keV.**

The comparison plots in Figure 41 simply depict how the “Buckyball” sputtering in TOF SIMS was effective in partially cleaning the surface of ThO<sub>2</sub>. The as-grown and polished

spectra at the low beam energy of 1.51 keV were achievable after TOF SIMS whereas when before TOF SIMS they were not.

#### 4.5 Optical Transmittance Spectrum

As has been explained, the deconvolution work strongly indicated that the  $\text{ThO}_2$  band gap is 5.1 eV; however, an absorption measurement confirmed that the absorption edge is indeed approximately 5.1 eV.

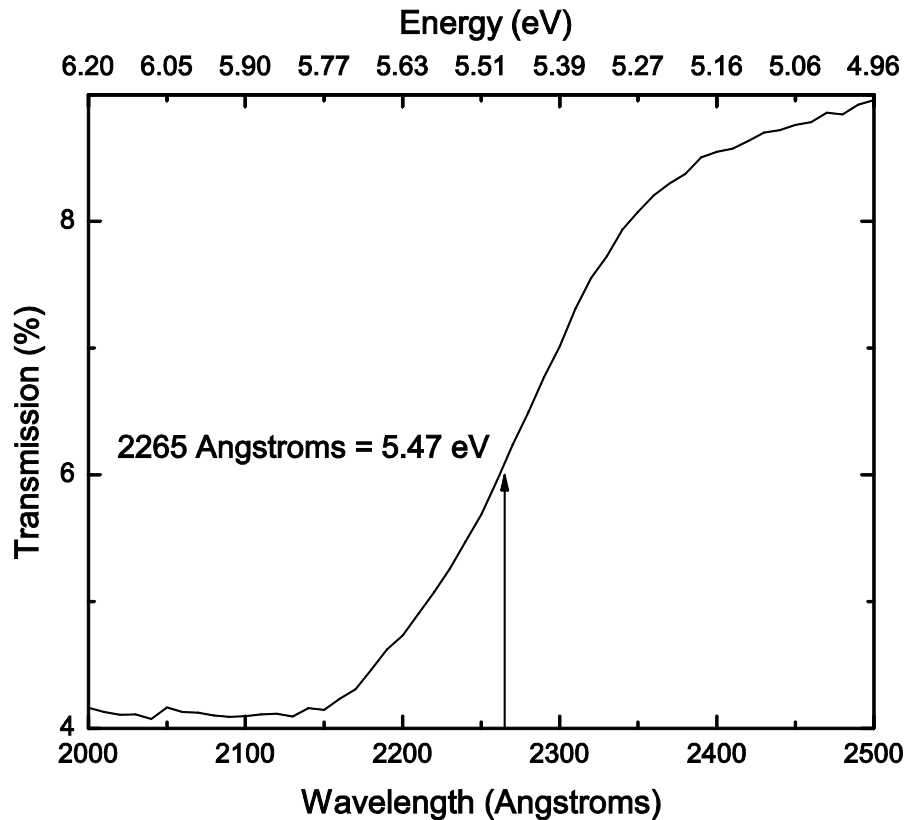


Figure 42. Optical Transmittance Spectrum at room temperature. Spectrum taken by Mr. Mike Ranft.

Figure 42's cut-off value of 2265 Å (or 5.4 eV) was determined by taking the derivative at each point on the data spectrum. The derivative at each point indicated the inflection point, where that inflection point was the absorption edge of this cleaved  $\text{ThO}_2$ . The



absorption measurement was conducted twice to demonstrate that this result was reproducible. The second run of the absorption spectrum for the polished sample was identical to the first run; therefore, the 5.4 eV absorption edge value can be taken with confidence. The six spectra taken of the as-grown sample proved not so helpful however. The as-grown sample was so thick that the light source could not accurately be detected by the spectrophotometer. Hence, the optical transmittance data for the as-grown sample cannot be taken with confidence and was not included in this report.

## V Conclusions and Recommendations for Future Research

### 5.1 CASINO

The ThO<sub>2</sub> crystals were modeled in an electron depth penetration program called CASINO. CASINO simulates with electrons at various beam energies to determine how far electrons will impinge in a material. The simulation was conducted for beam energies of 1-12 keV, and Table 2 provides the expected interaction depth. With this information, CL experiments were designed to investigate by probing from the surface of the material down to its bulk.

### 5.2 CL

Depth-resolved CL explored two different ThO<sub>2</sub> samples: as-grown and polished. TOF SIMS was conducted on these two samples. Prior to TOF SIMS, the as-grown spectra exhibited a dependency upon beam energy (variation of 1.5 – 12 keV) but not upon temperature. On the other hand, the polished sample exhibited little dependence upon beam energy (variation of 5 – 10 keV) but significant dependence upon temperature. TOF SIMS inadvertently partially “cleaned” the surface of the ThO<sub>2</sub> samples. After TOF SIMS, the as-grown sample had no variation in spectral shifts as beam energy was changed from 1.5 – 10 keV. The polished sample continued to exhibit little dependence upon beam energy. All spectra were deconvolved and peak fitted, which resulted the band gap value of 5.1 eV. An optical transmittance measurement indicated an absorption edge at 5.4 eV.

### 5.3 Recommendations for Future Research

First, a temperature variation study should be conducted to determine if TOF SIMS had an effect on the crystals. The ThO<sub>2</sub> crystals should then be chemically cleaned with ether, which should take all of the surface artifacts off. Followed by this, AFM measurements on the samples should be done to confirm that the surface elements are gone. Then, another detailed depth-resolved CL should be conducted in order to confirm the results and analyses in this report.

The ThO<sub>2</sub> crystals can be studied by electron paramagnetic resonance (EPR) to characterize some of the electronic defect structure of thorium. An unpaired electron can move between the two energy levels by either absorbing or emitting electromagnetic radiation of energy such that the resonance condition is obeyed. Attaining a better understanding of the electronic defects can help explain the radiative behavior of ThO<sub>2</sub> under CL.

Another possible future research is conducting an in-depth photoluminescence (PL) study. Having a detailed PL report to combine and compare with this depth-resolved CL study can confirm or deny any of the current findings. The PL measurements can be coupled with either SEM CL or profilometer (“Stylus”) so images of the surface of the material can be obtained while collecting CL data to complement the current surface and bulk findings.

## Appendix A

### CL Start-Up Procedure

The procedure to begin taking measurements on the CL system is detailed, where prior to mounting the sample  $\text{HfO}_2$ , the sample has to be cleaned with acetone (Dugan, 2011). A bead of vacuum grease attaches the sample to the CL sample holder. Also, a copper plate was placed above the samples to dissipate the electric charge build-up (Dugan, 2011). In the CL Lab at the Air Force Institute of Technology (AFIT), the start-up procedure is as follows (Dugan, 2011):

- A. Turn on the mechanical pump (keg fore pump) and then the turbomolecular pump to evacuate the system. Once the system with the sample in it is evacuated, bake the system down overnight.
  1. Ensure valve attached to the thin white tube under the table is on (in the up position)
  2. Turn on Alcatel (turbomolecular pump power)
  3. Ensure the plug on floor outlet behind chamber is plugged in
  4. Turn manual override switch (black box with switch on front) and the little button on outlet
  5. Wait until pressure drops to 100 on Ion Gauge Controller and Set Point 2 (SP2) and SP1 needs to be on.
  6. At  $9.9 \times 10^{-2}$  Torr turn off beeping switch when SP1 and SP2 lights come on
  7. Press start button on turbo pump
  8. Turn on ionization gauge after pressure is  $1.0 \times 10^{-3}$  Torr and turn has 27,000 RPMs.
  
- B. Cool chamber with liquid helium
  1. Turn on water valve which is the orange hose under table (up position)
  2. Turn on power, compressor, and then cold head switch on cooler behind table.
  3. Turn on Lakeshore temperature controller
  4. Wait for system to reach 7 K (~5 hours).
  
- C. Cool photomultiplier tube by switching knob on PMT housing control.
  
- D. Turn on electron gun power supply and electron gun
  1. First turn on electron gun high voltage power supply

2. Turn Voltage key, press power button, red HV switch, red source knob, blue deflection button
  3. Energy, focus, Source/ECC grid should be at zero.
  4. Function switch should be turned to energy and raise to desired energy.
- E. Turn on Keithley ammeter for gun and slowly raise current to 50  $\mu\text{A}$ , which is achieved with about 2.45 filament amps on electron gun power supply (this is also dependent on the beam energy).
1. To clear select I, local, zero check, auto.
- F. Open electron gun and watch current decrease to approximately 6  $\mu\text{A}$ .
- G. Turn on photomultiplier tube at Stanford Research System.
1. Cathode has 1200 Volts and anode is grounded.
- H. Ensure gun is aligned properly with sample. Turn off light to align luminescence from sample with spectrometer slit by adjusting the two optic lenses.
- I. Calibrate light from sample.
1. Turn on monitor
  2. Open SynerJV
  3. Press third button from right on top menu
  4. Select Hardware of 3000 Grating
  5. Enter dial reading on monochromator
  6. Select Data Scan and DSS and unchecked "active"
  7. Go to Data preview and uncheck continuous
  8. Select wavelength near desired wavelength and press play
  9. Adjust optics, x/y deflection knobs, and slit widths to gain optimal signal.
  10. Gradually lower slit widths to get maximum signal to noise ratio
  11. Once found highest signal at lowest slit width, return to main screen
- J. Run Sample.
1. Adjust slit widths and optics to maximize signal between iterations.
  2. Calibrate signal to noise ratio after each iteration.
  3. Save data & plot to check spectra.

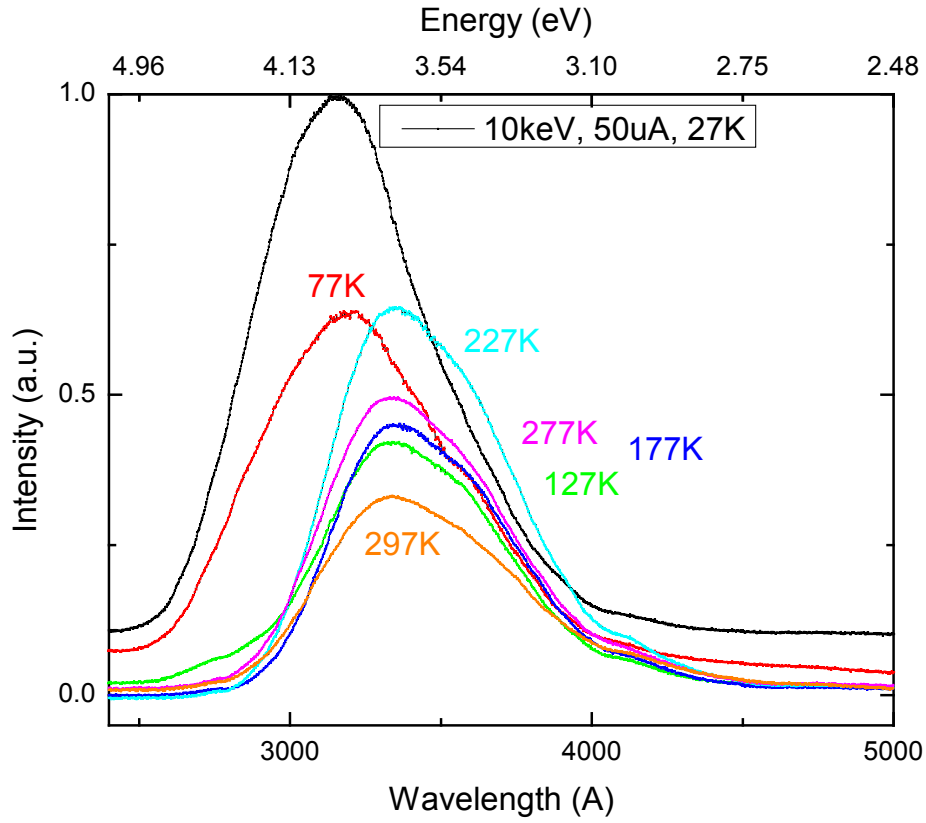
**The CL shut-down procedure is as follows (Dugan, 2011):**

- A. Warm chamber from liquid helium temperatures
1. Close liquid helium valve

2. Increase temperature on lakeshore controller to 300 K
  3. Turn off cold head, compressor, then power on cooler behind table
  4. Turn off water valve under table.
  5. Turn off Lakeshore temperature controller
- B. Warm photomultiplier tube
1. Switch off PMT Housing box (box will beep)
  2. Close valve to liquid nitrogen
  3. Turn off PMT Stanford Research Systems Controller
- C. Turn off electron gun
1. Turn down filament power with source button slowly counterclockwise
  2. Depress Red source switch
  3. Turn down grid voltage with grid potentiometer counterclockwise
  4. Turn down Energy and Focus potentiometers counterclockwise
  5. Depress the red H.V. switch
  6. Depress the power switch
  7. Turn key to off
  8. Turn off high voltage power source for gun
  9. Turn off Keithley ammeter for gun
- D. Turn off turbomolecular and roughing pump
1. Unplug the floor outlet which isolates the turbo pump from the roughing pump
  2. Select the stop button on Alcatel pump box
  3. Turn off the turbo pump power supply which will cause the rough pump to operate in air
  4. Turn off the second wall switch from right to turn off roughing pump

## Appendix B

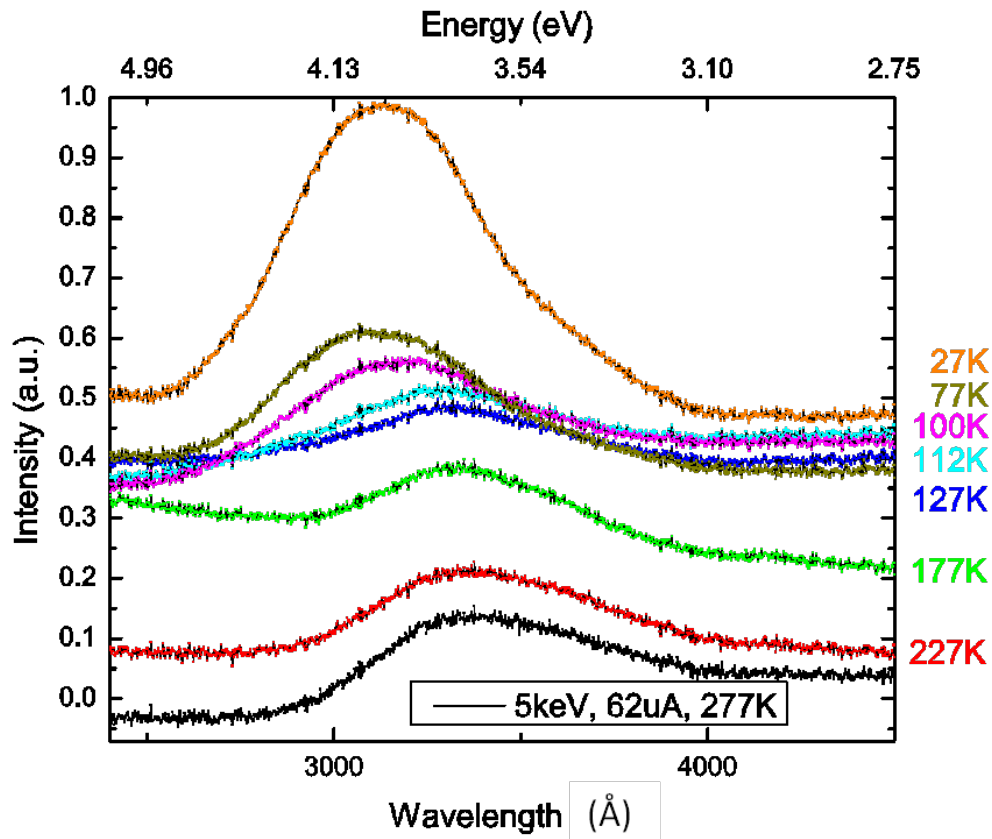
### ThO<sub>2</sub> Cleaved Sample, 10 keV Temperature Variation runs



Sample #004TO Temperature Dependent Peak Locations: 10keV, 50uA

Temperature [°K]	Location [Å]	Energy [eV]
27	3136	3.952
77	3178	3.9
100	3330	3.722
127	3362	3.686
177	3366	3.682
227	3366	3.682
277	3330	3.722
297	3358	3.691

ThO<sub>2</sub> Cleaved Sample, 5 keV Temperature Variation runs



Sample #004TO Temperature Dependent Peak Locations: 5keV, 62uA

Temperature [°K]	Location [Å]	Energy [eV]
27	3136	3.952
77	3172	3.907
100	3136	3.952
	3202	3.871
112	3276	3.783
127	3318	3.735
177	3376	3.671
227	3376	3.671
277	3376	3.671



## Bibliography

- Agilent Technologies. "Cary 5000 UV-Vis-NIR," 2013. 20 February 2013  
<http://www.chem.agilent.com/en-US/products-services/Instruments-Systems/Molecular-Spectroscopy/Cary-5000-UV-Vis-NIR/Pages/default.aspx#>.
- K. W. Bennett, N. Gupta, and R. Dahmani. "Development of In-House Grating Spectrometer System for Validating Acousto-Optic Tunable Filter Spectrometer Results." *Army Research Laboratory Report ARL-MR-495*, 2001. 1 January 2013 <http://www.arl.army.mil/arlreports/2001/ARL-MR-495.pdf>.
- A. Billeb, W. Grieshaber, D. Stocker, E. F. Schubert, and R. F. Karlicek, Jr.. "Microcavity effects in GaN epitaxial films and in Ag/GaN/sapphire structures." *Applied Physics Letters*, 70, no. 21 (1997): 2790-2792.
- J. Bolze, S. Rekhi, K. Macchiarola, B. Litterer. "Size Distribution Determination of Nanoparticles and Nanosized Pores by Small-Angle X-ray Scattering on a Multi-Purpose X-ray Diffractometer Platform." *Nanotech 2010: Technical Proceedings of the 2010 NSTI Nanotechnology Conference and Expo*, vol 1. Cambridge MA: Nanoscience and Technology Institute, 2010.
- D. K. Bowen and B. K. Tanner. *X-Ray Metrology in Semiconductor Manufacturing*, Boca Raton FL: Taylor & Francis Group, LLC, 2006.
- J. Castilow. MS Student, Department of Engineering Physics, Air Force Institute of Technology. Personal Interview. 31 December 2012.
- C. A. Colmenares. Unpublished Research. Lawrence Livermore National Laboratory, Livermore, CA, 1981.
- B. D. Cullity. *Elements of X-ray Diffraction*. Reading MA: Addison-Wesley, 1956.
- D. Drouin, A. R. Couture, D. Joly, X. Tastet, V. Aimez, and R. Gauvin. "CASINO V2.42—A Fast and Easy-to-use Modeling Tool for Scanning Electron Microscopy and Microanalysis Users." *Scanning*, 29 (2007): 92-101.
- C. L. Dugan. "Cathodoluminescence and photoemission of doped lithium tetraborate." MS Thesis, Air Force Institute of Technology, 2011.
- W.P. Ellis, A.M. Boring, J.W. Allen, L.E. Cox, R.D. Cowan, B.B. Pate, A.J. Arko, and I. Lindau. "Valance-Band photoemission intensities in thorium dioxide." *Solid State Communications*, 72, no. 7 (1989): 725-729.
- "Expanding the Frontiers of Science." (n.d.) 12 October 2012 <http://www.newport.com>.
- K. Fleischer, M. Toth, M. R. Philips, J. Zou, G. Li, and S. J. Chua. "Depth profiling of GaN by cathodoluminescence microanalysis." *Applied Physics Letters*, 74, no. 8 (1999): 1114-1116.

- “Fluorite-unit.” (19 March 2007). 23 December 2012  
<http://en.wikipedia.org/wiki/File:Fluorite-unit-cell-3D-ionic.png>.
- M. Fox. *Optical Properties of Solids*, 2 ed.. New York NY: Oxford University Press, 2010.
- W. A. Harrison. *Solid State Theory*. New York NY: McGraw-Hill, 1970.
- P. J. Harvey and J. B. Hallett. ”Factors Influencing the Photoluminescence Behavior of Thoria.” *Journal of the Electrochemical Society*, 123, no. 3 (1976): 398-403.
- P. J. Harvey, B. G. Childs, and J. Moerman. ”Optical Absorbance and Fluorescence in Pure and Doped ThO<sub>2</sub>.” *Journal of the American Ceramic Society*, 56, no. 3 (1973): 134-136.
- R. L. Hengehold. Course notes, “Optical Radiometry and Detection.” Department of Engineering Physics, Air Force Institute of Technology, Wright-Patterson AFB OH, 2012.
- “High Vacuum Products.” (n.d.) 26 December 2012  
[http://www.highervacuum.com/product/p4/Cold\\_heads.pdf](http://www.highervacuum.com/product/p4/Cold_heads.pdf).
- A. Holmes-Siedle and L. Adams. *Handbook of Radiation Effects*, 2 ed.. New York NY: Oxford University Press, 2002.
- “HORIBA Jobin Yvon Spectrometers.” (n.d.) 01 January 2013 <http://www.horiba.com/>.
- “ICSD.” (n.d.) 01 January 2013, <http://www.fiz-karlsruhe.com/icsd.html>.
- A. M. Kiefer. Wright-Patterson Air Force Base. Personal Interview. 2 October 2012.  
 ----- Personal Interview. 12 October 2012.
- “EGG-3013/EGPS-3103.” (n.d.) 1 December 2012 <http://www.kimballphysics.com/electron-gun-systems/electron-gun-products/medium-energy/egg-3103-egps-3103>.
- Kimball Physics, Inc.. *Operator’s Manual: EMG-12/EGPS-12 Electron Gun and Power Supply*. Wilton NH: Kimball Physics, Inc., 1999.
- G. F. Knoll. *Radiation Detection and Measurement*, 4 ed.. New York NY: Wiley, 2010.
- T.R.G. Kutty, M.R. Nair, P. Sengupta, U. Basak, Arun Kumar, and H.S. Kamath. “Characterization of (Th,U)O<sub>2</sub> fuel pellets made by impregnation technique.” *Journal of Nuclear Materials*, 374 (2008): 9-19.
- Y. Liao. “Practical Electron Microscopy and Database.” (4 March 2012) 1 September 2012 <http://www.globalsino.com/EM/page4832.html>.
- M. D. Lumb. *Luminescence Spectroscopy*. New York NY: Academic Press, 1978.

- R. Maitura. *Nuclear Reports* (2005): 46-53.
- M. Mann. “Hydrothermal Crystal Growth of Tetravalent and Pentavalent Metal Oxides.” PhD dissertation, Clemson University, 2009.
- M. Mann, D. Thompson, K. Serivalsatit, T. M. Tritt, J. Ballato, and J. Kolis. “Hydrothermal Growth and Thermal Property Characterization of ThO<sub>2</sub> Single Crystals.” *Crystal Growth & Design*, 10, no. 5 (2010): 2146-2151.
- P. Martin, D. J. Cooke, and R. Cywinski. “A molecular dynamics study of the thermal properties of thorium oxide.” *Journal of Applied Physics*, 112, 073507 (2012).
- J. P. McKelvey. *Solid State Physics for Engineering and Materials Science*. Malabar FL: Krieger Publishing Company, 1993.
- “MSeries.” (n.d.) 26 December 2012, <http://www.horiba.com/fileadmin/uploads/Scientific/Documents/OSD/MSeries.pdf>.
- V. I. Neeley, J. B. Gruber, and W. J. Gray. “F Centers in Thorium Oxide.” *Physical Review*, 158, no. 3 (1967): 809-813.
- K. Nomura, H. Ohta, K. Ueda, T. Kamiya, M. Hirano, and H. Hosono. “Thin-Film Transistor Fabricated in Single-Crystalline Transparent Oxide Semiconductor.” *Science*, 300, no. 5623 (2003): 1269-1272.
- L. Ozawa. *Cathodoluminescence: Theory and Applications*. New York NY: VCH Publishers, 1990.
- “PANalytical.” (n.d.) 2 October 2012 <http://www.panalytical.com/index.cfm?pid=135>.
- “Products for Research, Inc.” (n.d.). 26 December 2012 <http://www.photocool.com/tocool.htm>.
- “Photocool Products.” (n.d.) 26 December 2012 <http://www.photocool.com/>.
- T. R. Saranathan, V. A. Fassel, and E. L. DeKalb. “Analytical applications of x-ray excited optical fluorescence spectra. Direct determination of fractional parts per million amounts of rare earths in thorium.” *Analytical Chemistry*, 42, no. 3 (1970): 325-329.
- B. D. Saksena and L. M. Pant. “Cathodo-Luminescence of MgO.” *Proceedings of the Physical Society. Section B*, 67, no. 11 (1954): 811-816.
- B. W. Schueler. “Microscope imaging by time-of-flight secondary ion mass spectrometry.” *Microscopy Microanalysis Microstructures*, 3, no. 2-3 (1992): 119-139.
- SPECS GmbH. *CCX 60 Water Cooling Unit*. Berlin: SPECS GmbH, 2009.

- “SynerJY.” (n.d.) 26 December 2012, <http://www.horiba.com/scientific/products/optical-spectroscopy/software/synerjy/>.
- S. M. Sze. *Semiconductor Devices*, 2 ed.. New York NY: John Wiley & Sons, 2002.
- B. Szpunar and J.A. Szpunar. (n.d.) 2012 “Application of density functional theory in assessing properties of thorium and recycled fuels.” *Journal of Nuclear Materials*, in press. Available online at <http://www.sciencedirect.com/science/article/pii/S0022311512005259>.
- R. Terki, H. Feraoun, G. Bertrand, and H. Aourag. “First principles calculations of structural, elastic and electronic properties of XO<sub>2</sub> (X = Zr, Hf and Th) in fluorite phase.” *Computational Materials Science*, 33, no. 1-3 (2005): 44-52.
- “Thorium.” (n.d.). 23 December 2012, [http://en.wikipedia.org/wiki/Thorium\\_fuel\\_cycle](http://en.wikipedia.org/wiki/Thorium_fuel_cycle).
- D. R. Vij. *Luminescence of Solids*. New York NY: Plenum Press, 1998.
- R. E. Viturro, J. L. Shaw, L. J. Brillson, J. M. Woodall, P. D. Kirchner, G. D. Pettit, and S. L. Wright. “Arsenic- and metal-induced GaAs interface states by low-energy cathodoluminescence spectroscopy.” *Journal of Vacuum Science & Technology B*, 6, no. 4 (1988): 1397-1402.
- R.W. Vook, C.A. Colmenares, R.L. Smith, and R.G. Gutmacher. “Cathodoluminescence of thorium in the presence of O<sub>2</sub>, CO and gas mixtures of CO-O<sub>2</sub> and CO-H<sub>2</sub>.” *Journal of Luminescence*, 27, no. 2 (1982): 115-126.
- B. T. Wang, H. Shi, W.-D. Li, and P. Zhang. “First-principles study of ground-state properties and high pressure behavior of ThO<sub>2</sub>.” *Journal of Nuclear Materials*, 399, no. 2-3 (2010): 181-188.
- H. Yamamoto. “Atomic Force Microscope.” *United States Patent*, US 5,406,833 (18 April 1995).
- M. Yoshikawa, K. Matsuda, Y. Yamaguchi, T. Matsunobe, Y. Nagasawa, H. Fujino, and T. Yamane. “Characterization of silicon dioxide film by high spatial resolution cathodoluminescence spectroscopy.” *Journal of Applied Physics*, 92, no. 12 (2002): 7153-7156.

## Vita

Major Michael G. Lee commissioned in the Infantry, from the United States Military Academy in 2002, with a Bachelor of Science degree in Civil Engineering. He served as a Rifle Platoon Leader, Executive Officer, and Air Operations Officer in 3rd Battalion, 504th Parachute Infantry Regiment, 82nd Airborne Division at FT Bragg, North Carolina.

In December of 2003, MAJ Lee deployed to Balad, Iraq as a Rifle Platoon Leader in support of Operation Iraqi Freedom 3. MAJ Lee served as a Rifle Company Executive Officer from August 2004 through August 2005. He became the S-3 AIR in August 2005, and he deployed 3-504th PIR to Al Asad, Iraq in support of Operation Iraqi Freedom 6. After completing the Infantry Captains Career Course and the Mechanized Leader Course in 2006, MAJ Lee reported for duty at 1-72 Armor Combined Arms Battalion, to serve as the Battalion S-4 for seven months and Mechanized Infantry Rifle Company Commander for 17 months.

On 12 January 2009, MAJ Lee assumed command of Headquarters and Headquarters Company, 4<sup>th</sup> Ranger Training Battalion at FT Benning, GA. He served there for 18 months supporting the training of Ranger leaders and trained the company's opposition force Infantry Platoons and medics in preparation for their follow-on assignments after duty at 4<sup>th</sup> Ranger Training Battalion.

MAJ Lee's awards and decorations include the Combat Infantryman Badge, Expert Infantryman Badge, Ranger Tab, Senior Parachutist Badge, the Bronze Star Medal, Meritorious Service Medal with 1 oak leaf cluster, Army Commendation Medal (1OLC), Army Achievement Medal (1 OLC), Iraq Service Medal, Global War on Terrorism Expeditionary Medal, and other service medals and service ribbons. MAJ Lee's next assignment will be at the Defense Intelligence Agency—Counter-Proliferation and Terrorism—in Charlottesville, VA.

MAJ Lee is a native of Colorado Springs, Colorado. He is married and blessed with three children.

<b>REPORT DOCUMENTATION PAGE</b>				<i>Form Approved OMB No. 074-0188</i>	
<p>The public reporting burden for this collection of information is estimated to average 1 hour per response, including the time for reviewing instructions, searching existing data sources, gathering and maintaining the data needed, and completing and reviewing the collection of information. Send comments regarding this burden estimate or any other aspect of the collection of information, including suggestions for reducing this burden to Department of Defense, Washington Headquarters Services, Directorate for Information Operations and Reports (0704-0188), 1215 Jefferson Davis Highway, Suite 1204, Arlington, VA 22202-4302. Respondents should be aware that notwithstanding any other provision of law, no person shall be subject to a penalty for failing to comply with a collection of information if it does not display a currently valid OMB control number.</p> <p><b>PLEASE DO NOT RETURN YOUR FORM TO THE ABOVE ADDRESS.</b></p>					
<b>1. REPORT DATE</b> (DD-MM-YYYY) <i>GF</i>		<b>2. REPORT TYPE</b>		<b>3. DATES COVERED</b> (From – To)	
43-03-2013		Master's Thesis		June 2011 - March 2013	
<b>TITLE AND SUBTITLE</b>				<b>5a. CONTRACT NUMBER</b>	
Depth-Resolved Cathodoluminescence of ThO <sub>2</sub>				<b>5b. GRANT NUMBER</b>	
				<b>5c. PROGRAM ELEMENT NUMBER</b>	
<b>6. AUTHOR(S)</b>				<b>5d. PROJECT NUMBER</b>	
Lee, Michael G., Major, USA				<b>5e. TASK NUMBER</b>	
				<b>5f. WORK UNIT NUMBER</b>	
<b>7. PERFORMING ORGANIZATION NAMES(S) AND ADDRESS(S)</b>				<b>8. PERFORMING ORGANIZATION REPORT NUMBER</b>	
Air Force Institute of Technology Graduate School of Engineering and Management (AFIT/ENP) 2950 Hobson Way, Building 640 WPAFB OH 45433-7765				AFIT-ENP-13-M-21	
<b>9. SPONSORING/MONITORING AGENCY NAME(S) AND ADDRESS(ES)</b>				<b>10. SPONSOR/MONITOR'S ACRONYM(S) DHS/DNDO</b>	
Department of Homeland Defense, Domestic Nuclear Detection Office Samantha Kentis 245 Murray Lane SW Washington, DC 20407				<b>11. SPONSOR/MONITOR'S REPORT NUMBER(S)</b>	
<b>12. DISTRIBUTION/AVAILABILITY STATEMENT</b> APPROVED FOR PUBLIC RELEASE; DISTRIBUTION UNLIMITED. DISTRIBUTION STATEMENT A.					
<b>13. SUPPLEMENTARY NOTES</b>					
<b>14. ABSTRACT</b>					
<p>Single crystal thorium dioxide (ThO<sub>2</sub>) samples were hydrothermally grown and studied using depth-resolved cathodoluminescence (CL) to characterize the surface and bulk electronic states. X-ray diffraction (XRD) measurements were collected to confirm that these crystals were ThO<sub>2</sub> in the fluorite structure. Understanding the chemical and structural quality of ThO<sub>2</sub> will aid in the fabrication of better neutron detectors as well as in the power production with thorium breeder reactors.</p> <p>Monte Carlo simulations predicted the expected energy-dependent electron interaction depths in the ThO<sub>2</sub> crystals. CL was conducted with electron energy range of 1.5 - 12 keV, a current range of 30-62 μA, at pressures of 5×10<sup>-7</sup> to 1.2×10<sup>-9</sup> Torr, and temperatures of 24 K – 297 K. The initial CL measurements indicated that the as-grown sample exhibited more of an energy dependency than the cleaved sample. Time of flight secondary ion mass spectrometry (TOF SIMS) was conducted on the samples, which cleaned the surface. Additional CL measurements were conducted on both samples, which showed that the as-grown sample no longer had an energy dependency.</p> <p>With the CL results and peak deconvolutions, it is compelling to believe that the absorption edge is 5.1 eV, which is complemented with the absorption measurement of 5.4 eV.</p>					
<b>15. SUBJECT TERMS</b> Thorium Dioxide, Depth-Resolved Cathodoluminescence, absorption edge, hydrothermal growth method.					
<b>16. SECURITY CLASSIFICATION OF:</b>			<b>17. LIMITATION OF ABSTRACT</b>	<b>18. NUMBER OF PAGES</b>	<b>19a. NAME OF RESPONSIBLE PERSON</b>
<b>a. REPORT</b>	<b>b. ABSTRACT</b>	<b>c. THIS PAGE</b>			Dr. Robert L. Hengehold (AFIT/ENP)
U	U	U	UU	93	<b>19b. TELEPHONE NUMBER (Include area code)</b> (937) 477-8787, ext 4502 (robert.hengehold@afit.edu)

Standard Form 298 (Rev. 8-98)  
Prescribed by ANSI Std. Z39-18